12-week treatment, suggesting that 1C2 immunostaining of scrotal skin biopsy samples for nuclear mutant AR is a practical procedure for estimating the severity of SBMA pathogenesis in the nervous system [80]. Based on the observations described above, the degree of 1C2-stained nuclear mutant AR accumulation in biopsied scrotal skin is likely to be a potent biomarker reflecting the pathogenic process of SBMA. Since the degree of nuclear accumulation of mutant AR in biopsied scrotal skin appears to be a promising surrogate endpoint, further trials are necessary to evaluate this biomarker by confirming that the change in scrotal skin findings correctly predicts the true clinical outcome event such as becoming wheelchair-bound, aspiration pneumonia or death.

Conclusions

Studies using cellular and animal models provide insight into mechanisms involved in neurodegeneration in SBMA, and reveal promising approaches to treatment of this disease, among which LHRH analogues and 17-AAG appear to be potent agents for treating patients. The results of animal studies should be verified in carefully designed clinical trials. Clinical studies on SBMA patients, however, are challenging because of the slowly progressive nature of SBMA and the low sensitivity of clinical examination to detect changes over short periods of time. Furthermore, these treatments for SBMA are disease-modifying therapies that inhibit the pathogenic process of motor neurone degeneration rather than symptom-relief therapies (Figure 3). Therefore, large-scale clinical trials of long duration are necessary, and establishment of objective biomarkers is of utmost importance in order to improve the power and cost-effectiveness of longitudinal clinical treatment trials (Figure 3). For this purpose, clinical and pathological parameters representing the pathogenic process of SBMA should be extensively investigated.

The ideal treatment for polyQ diseases appears to be a combination of several potential therapeutic strategies, as each approach has adverse effects and long-term treatment is unavoidable in the therapy of polyQ diseases. Elucidation of the pathophysiology, high-throughput drug screening and intensive clinical trials are necessary for establishing human therapeutics for this disease.

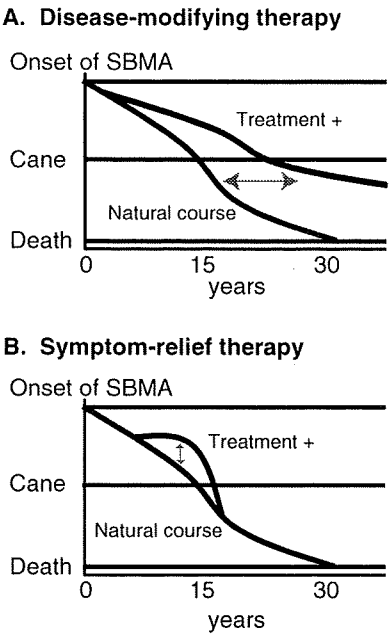

Figure 3. Disease-modifying and symptom-relief therapies for spinal and bulbar muscular atrophy (SBMA). (A) Long-term clinical trials are necessary to evaluate the effects of disease-modifying therapies, as SBMA is a slowly progressive disease. (B) Symptom-relief therapy ameliorates symptoms of SBMA, and the duration of these clinical trials is short. The *y*-axis shows the general clinical course of SBMA patients. 'Cane' indicates the requirement of a cane for walking. Arrows indicate the study duration that is required for each therapy.

Acknowledgements

We thank the National Cancer Institute and Kosan Biosciences for kindly providing 17-AAG. This work was supported by a Center-of-Excellence (COE) grant and KAKENHI (17025020) from the Ministry of Education, Culture, Sports, Science and Technology, Japan, grants from the Ministry of Health, Labour and Welfare, Japan, a grant from the Naito Foundation, and a grant from the Kanae Foundation.

References

1 Takahashi A. Hiroshi Kawahara (1858–1918). *J Neurol* 2001; **248**: 241–2
2 Kawahara H. A family of progressive bulbar palsy. *Aichi Med J* 1897; **16**: 3–4
3 Kennedy WR, Alter M, Sung JH. Progressive proximal spinal and bulbar muscular atrophy of late onset. A sex-linked recessive trait. *Neurology* 1968; **18**: 671–80
4 La Spada AR, Wilson EM, Lubahn DB, Harding AE, Fischbeck KH. Androgen receptor gene mutations in X-linked spinal and bulbar muscular atrophy. *Nature* 1991; **352**: 77–9
5 Di Prospero NA, Fischbeck KH. Therapeutics development for triplet repeat expansion diseases. *Nat Rev Genet* 2005; **6**: 756–65

6 Sobue G, Hashizume Y, Mukai E, Hirayama M, Mitsuma T, Takahashi A. X-linked recessive bulbospinal neuronopathy. A clinicopathological study. *Brain* 1989; **112**: 209–32
7 Lee JH, Shin JH, Park KP, Kim IJ, Kim CM, Lim JG, Choi YC, Kim DS. Phenotypic variability in Kennedy's disease: implication of the early diagnostic features. *Acta Neurol Scand* 2005; **112**: 57–63
8 Atsuta N, Watanabe H, Ito M, Banno H, Suzuki K, Katsuno M, Tanaka F, Tamakoshi A, Sobue G. Natural history of spinal and bulbar muscular atrophy (SBMA). A study of 223 Japanese patients. *Brain* 2006; **129**: 1446–55
9 Arbizu T, Santamaria J, Gomez JM, Quilez A, Serra JP. A family with adult spinal and bulbar muscular atrophy, X-linked inheritance and associated testicular failure. *J Neurol Sci* 1983; **59**: 371–82
10 Hausmanowa-Petrusewicz I, Borkowska J, Janczewski Z. X-linked adult form of spinal muscular atrophy. *J Neurol* 1983; **229**: 175–88
11 Nagashima T, Seko K, Hirose K, Mannen T, Yoshimura S, Arima R, Nagashima K, Morimatsu Y. Familial bulbospinal muscular atrophy associated with testicular atrophy and sensory neuropathy (Kennedy–Alter–Sung syndrome). Autopsy case report of two brothers. *J Neurol Sci* 1988; **87**: 141–52
12 Echaniz-Laguna A, Rousso E, Anheim M, Cossee M, Tranchant C. A family with early-onset and rapidly progressive X-linked spinal and bulbar muscular atrophy. *Neurology* 2005; **64**: 1458–60
13 Danek A, Witt TN, Mann K, Schweikert HU, Romalo G, La Spada AR, Fischbeck KH. Decrease in androgen binding and effect of androgen treatment in a case of X-linked bulbospinal neuronopathy. *Clin Invest* 1994; **72**: 892–7
14 Goldenberg JN, Bradley WG. Testosterone therapy and the pathogenesis of Kennedy's disease (X-linked bulbospinal muscular atrophy). *J Neurol Sci* 1996; **135**: 158–61
15 Neuschmid-Kaspar F, Gast A, Peterziel H, Schneikert J, Muigg A, Ransmayr G, Klocker H, Bartsch G, Cato AC. CAG-repeat expansion in androgen receptor in Kennedy's disease is not a loss of function mutation. *Mol Cell Endocrinol* 1996; **117**: 149–56
16 Antonini G, Gragnani F, Romaniello A, Pennisi EM, Morino S, Ceschin V, Santoro L, Cruccu G. Sensory involvement in spinal-bulbar muscular atrophy (Kennedy's disease). *Muscle Nerve* 2000; **23**: 252–8
17 Lieberman AP, Fischbeck KH. Triplet repeat expansion in neuromuscular disease. *Muscle Nerve* 2000; **23**: 843–50
18 Sinnreich M, Sorenson EJ, Klein CJ. Neurologic course, endocrine dysfunction and triplet repeat size in spinal bulbar muscular atrophy. *Can J Neurol Sci* 2004; **31**: 378–82
19 Schmidt BJ, Greenberg CR, Allingham-Hawkins DJ, Spriggs EL. Expression of X-linked bulbospinal muscular atrophy (Kennedy disease) in two homozygous women. *Neurology* 2002; **59**: 770–2
20 Sobue G, Doyu M, Kachi T, Yasuda T, Mukai E, Kumagai T, Mitsuma T. Subclinical phenotypic expressions in heterozygous females of X-linked recessive bulbospinal neuronopathy. *J Neurol Sci* 1993; **117**: 74–8
21 Greenland KJ, Zajac JD. Kennedy's disease: pathogenesis and clinical approaches. *Intern Med J* 2004; **34**: 279–86
22 Mariotti C, Castellotti B, Pareyson D, Testa D, Eoli M, Antozzi C, Silani V, Marconi R, Tezzon F, Siciliano G, Marchini C, Gellera C, Donato SD. Phenotypic manifestations associated with CAG-repeat expansion in the androgen receptor gene in male patients and heterozygous females: a clinical and molecular study of 30 families. *Neuromuscul Disord* 2000; **10**: 391–7
23 Sperfeld AD, Karitzky J, Brummer D, Schreiber H, Haussler J, Ludolph AC, Hanemann CO. X-linked bulbospinal neuronopathy: Kennedy disease. *Arch Neurol* 2002; **59**: 1921–6
24 Poletti A. The polyglutamine tract of androgen receptor: from functions to dysfunctions in motor neurons. *Front Neuroendocrinol* 2004; **25**: 1–26
25 Benten WP, Lieberherr M, Stamm O, Wrehlke C, Guo Z, Wunderlich F. Testosterone signaling through internalizable surface receptors in androgen receptor-free macrophages. *Mol Biol Cell* 1999; **10**: 3113–23
26 Lutz LB, Jamnongjit M, Yang WH, Jahani D, Gill A, Hammes SR. Selective modulation of genomic and nongenomic androgen responses by androgen receptor ligands. *Mol Endocrinol* 2003; **17**: 1106–16
27 Walker WH. Nongenomic actions of androgen in Sertoli cells. *Curr Top Dev Biol* 2003; **56**: 25–53
28 Ntais C, Polycarpou A, Tsatsoulis A. Molecular epidemiology of prostate cancer: androgens and polymorphisms in androgen-related genes. *Eur J Endocrinol* 2003; **149**: 469–77
29 Tanaka F, Doyu M, Ito Y, Matsumoto M, Mitsuma T, Abe K, Aoki M, Itoyama Y, Fischbeck KH, Sobue G. Founder effect in spinal and bulbar muscular atrophy (SBMA). *Hum Mol Genet* 1996; **5**: 1253–7
30 Tanaka F, Reeves MF, Ito Y, Matsumoto M, Li M, Miwa S, Inukai A, Yamamoto M, Doyu M, Yoshida M, Hashizume Y, Terao S, Mitsuma T, Sobue G. Tissue-specific somatic mosaicism in spinal and bulbar muscular atrophy is dependent on CAG-repeat length and androgen receptor – gene expression level. *Am J Hum Genet* 1999; **65**: 966–73
31 La Spada AR, Roling DB, Harding AE, Warner CL, Spiegel R, Hausmanowa-Petrusewicz I, Yee WC, Fischbeck KH. Meiotic stability and genotype-phenotype correlation of the trinucleotide repeat in X-linked spinal and bulbar muscular atrophy. *Nat Genet* 1992; **2**: 301–4

32 Igarashi S, Tanno Y, Onodera O, Yamazaki M, Sato S, Ishikawa A, Miyatani N, Nagashima M, Ishikawa Y, Sahashi K, Ibi T, Miyatake T, Tsuji S. Strong correlation between the number of CAG repeats in androgen receptor genes and the clinical onset of features of spinal and bulbar muscular atrophy. *Neurology* 1992; **42**: 2300–2

33 Doyu M, Sobue G, Mukai E, Kachi T, Yasuda T, Mitsuma T, Takahashi A. Severity of X-linked recessive bulbospinal neuronopathy correlates with size of the tandem CAG repeat in androgen receptor gene. *Ann Neurol* 1992; **32**: 707–10

34 Shimada N, Sobue G, Doyu M, Yamamoto K, Yasuda T, Mukai E, Kachi T, Mitsuma T. X-linked recessive bulbospinal neuronopathy: clinical phenotypes and CAG repeat size in androgen receptor gene. *Muscle Nerve* 1995; **18**: 1378–84

35 Katsuno M, Adachi H, Kume A, Li M, Nakagomi Y, Niwa H, Sang C, Kobayashi Y, Doyu M, Sobue G. Testosterone reduction prevents phenotypic expression in a transgenic mouse model of spinal and bulbar muscular atrophy. *Neuron* 2002; **35**: 843–54

36 Takeyama K, Ito S, Yamamoto A, Tanimoto H, Furutani T, Kanuka H, Miura M, Tabata T, Kato S. Androgen-dependent neurodegeneration by polyglutamine-expanded human androgen receptor in Drosophila. *Neuron* 2002; **35**: 855–64

37 Katsuno M, Adachi H, Doyu M, Minamiyama M, Sang C, Kobayashi Y, Inukai A, Sobue G. Leuprorelin rescues polyglutamine-dependent phenotypes in a transgenic mouse model of spinal and bulbar muscular atrophy. *Nat Med* 2003; **9**: 768–73

38 Sobue G, Matsuoka Y, Mukai E, Takayanagi T, Sobue I, Hashizume Y. Spinal and cranial motor nerve roots in amyotrophic lateral sclerosis and X-linked recessive bulbospinal muscular atrophy: morphometric and teased-fiber study. *Acta Neuropathol (Berl)* 1981; **55**: 227–35

39 Li M, Sobue G, Doyu M, Mukai E, Hashizume Y, Mitsuma T. Primary sensory neurons in X-linked recessive bulbospinal neuropathy: histopathology and androgen receptor gene expression. *Muscle Nerve* 1995; **18**: 301–8

40 Guidetti D, Vescovini E, Motti L, Ghidoni E, Gemignani F, Marbini A, Patrosso MC, Ferlini A, Solime F. X-linked bulbar and spinal muscular atrophy, or Kennedy disease: clinical, neurophysiological, neuropathological, neuropsychological and molecular study of a large family. *J Neurol Sci* 1996; **135**: 140–8

41 Li M, Miwa S, Kobayashi Y, Merry DE, Yamamoto M, Tanaka F, Doyu M, Hashizume Y, Fischbeck KH, Sobue G. Nuclear inclusions of the androgen receptor protein in spinal and bulbar muscular atrophy. *Ann Neurol* 1998; **44**: 249–54

42 Li M, Nakagomi Y, Kobayashi Y, Merry DE, Tanaka F, Doyu M, Mitsuma T, Hashizume Y, Fischbeck KH, Sobue G. Nonneural nuclear inclusions of androgen receptor protein in spinal and bulbar muscular atrophy. *Am J Pathol* 1998; **153**: 695–701

43 Kobayashi Y, Miwa S, Merry DE, Kume A, Mei L, Doyu M, Sobue G. Caspase-3 cleaves the expanded androgen receptor protein of spinal and bulbar muscular atrophy in a polyglutamine repeat length-dependent manner. *Biochem Biophys Res Commun* 1998; **252**: 145–50

44 Ellerby LM, Hackam AS, Propp SS, Ellerby HM, Rabizadeh S, Cashman NR, Trifiro MA, Pinsky L, Wellington CL, Salvesen GS, Hayden MR, Bredesen DE. Kennedy's disease: caspase cleavage of the androgen receptor is a crucial event in cytotoxicity. *J Neurochem* 1999; **72**: 185–95

45 Tanaka M, Machida Y, Nishikawa Y, Akagi T, Hashikawa T, Fujisawa T, Nukina N. Expansion of polyglutamine induces the formation of quasi-aggregate in the early stage of protein fibrillization. *J Biol Chem* 2003; **278**: 34717–24

46 Tanaka M, Morishima I, Akagi T, Hashikawa T, Nukina N. Intra- and intermolecular beta-pleated sheet formation in glutamine-repeat inserted myoglobin as a model for polyglutamine diseases. *J Biol Chem* 2001; **276**: 45470–5

47 Michalik A, Van Broeckhoven C. Pathogenesis of polyglutamine disorders: aggregation revisited. *Hum Mol Genet* 2003; **12**: R173–86

48 Simeoni S, Mancini MA, Stenoien DL, Marcelli M, Weigel NL, Zanisi M, Martini L, Poletti A. Motoneuronal cell death is not correlated with aggregate formation of androgen receptors containing an elongated polyglutamine tract. *Hum Mol Genet* 2000; **9**: 133–44

49 Bates G. Huntingtin aggregation and toxicity in Huntington's disease. *Lancet* 2003; **361**: 1642–4

50 Walcott JL, Merry DE. Trinucleotide repeat disease. The androgen receptor in spinal and bulbar muscular atrophy. *Vitam Horm* 2002; **65**: 127–47

51 Ross CA, Poirier MA, Wanker EE, Amzel M. Polyglutamine fibrillogenesis: the pathway unfolds. *Proc Natl Acad Sci USA* 2003; **100**: 1–3

52 Arrasate M, Mitra S, Schweitzer ES, Segal MR, Finkbeiner S. Inclusion body formation reduces levels of mutant huntingtin and the risk of neuronal death. *Nature* 2004; **431**: 805–10

53 Bowman AB, Yoo SY, Dantuma NP, Zoghbi HY. Neuronal dysfunction in a polyglutamine disease model occurs in the absence of ubiquitin-proteasome system impairment and inversely correlates with the degree of nuclear inclusion formation. *Hum Mol Genet* 2005; **14**: 679–91

54 Rusmini P, Sau D, Crippa V, Palazzolo I, Simonini F, Onesto E, Martini L, Poletti A. Aggregation and proteasome. The case of elongated polyglutamine aggregation in spinal and bulbar muscular atrophy. *Neurobiol Aging* 2006; doi: 10.1016/j.neurobiolaging.2006.05.015

55 Klement IA, Skinner PJ, Kaytor MD, Yi H, Hersch SM, Clark HB, Zoghbi HY, Orr HT. Ataxin-1 nuclear localization and aggregation: role in polyglutamine-induced disease in SCA1 transgenic mice. *Cell* 1998; **95**: 41–53

56 Saudou F, Finkbeiner S, Devys D, Greenberg ME. Huntingtin acts in the nucleus to induce apoptosis but death does not correlate with the formation of intranuclear inclusions. *Cell* 1998; **95**: 55–66
57 Yamada M, Wood JD, Shimohata T, Hayashi S, Tsuji S, Ross CA, Takahashi H. Widespread occurrence of intranuclear atrophin-1 accumulation in the central nervous system neurons of patients with dentatorubral-pallidoluysian atrophy. *Ann Neurol* 2001; **49**: 14–23
58 Adachi H, Katsuno M, Minamiyama M, Waza M, Sang C, Nakagomi Y, Kobayashi Y, Tanaka F, Doyu M, Inukai A, Yoshida M, Hashizume Y, Sobue G. Widespread nuclear and cytoplasmic accumulation of mutant androgen receptor in SBMA patients. *Brain* 2005; **128**: 659–70
59 Sapp E, Schwarz C, Chase K, Bhide PG, Young AB, Penney J, Vonsattel JP, Aronin N, DiFiglia M. Huntingtin localization in brains of normal and Huntington's disease patients. *Ann Neurol* 1997; **42**: 604–12
60 Garden GA, Libby RT, Fu YH, Kinoshita Y, Huang J, Possin DE, Smith AC, Martinez RA, Fine GC, Grote SK, Ware CB, Einum DD, Morrison RS, Ptacek LJ, Sopher BL, La Spada AR. Polyglutamine-expanded ataxin-7 promotes non-cell-autonomous purkinje cell degeneration and displays proteolytic cleavage in ataxic transgenic mice. *J Neurosci* 2002; **22**: 4897–905
61 Watase K, Weeber EJ, Xu B, Antalffy B, Yuva-Paylor L, Hashimoto K, Kano M, Atkinson R, Sun Y, Armstrong DL, Sweatt JD, Orr HT, Paylor R, Zoghbi HY. A long CAG repeat in the mouse Sca1 locus replicates SCA1 features and reveals the impact of protein solubility on selective neurodegeneration. *Neuron* 2002; **34**: 905–19
62 Yoo SY, Pennesi ME, Weeber EJ, Xu B, Atkinson R, Chen S, Armstrong DL, Wu SM, Sweatt JD, Zoghbi HY. SCA7 knockin mice model human SCA7 and reveal gradual accumulation of mutant ataxin-7 in neurons and abnormalities in short-term plasticity. *Neuron* 2003; **37**: 383–401
63 Steffan JS, Kazantsev A, Spasic-Boskovic O, Greenwald M, Zhu YZ, Gohler H, Wanker EE, Bates GP, Housman DE, Thompson LM. The Huntington's disease protein interacts with p53 and CREB-binding protein and represses transcription. *Proc Natl Acad Sci USA* 2000; **97**: 6763–8
64 Nucifora FC Jr, Sasaki M, Peters MF, Huang H, Cooper JK, Yamada M, Takahashi H, Tsuji S, Troncoso J, Dawson VL, Dawson TM, Ross CA. Interference by huntingtin and atrophin-1 with cbp-mediated transcription leading to cellular toxicity. *Science* 2001; **291**: 2423–8
65 Huynh DP, Yang HT, Vakharia H, Nguyen D, Pulst SM. Expansion of the polyQ repeat in ataxin-2 alters its Golgi localization, disrupts the Golgi complex and causes cell death. *Hum Mol Genet* 2003; **12**: 1485–96
66 Yamada M, Tsuji S, Takahashi H. Involvement of lysosomes in the pathogenesis of CAG repeat diseases. *Ann Neurol* 2002; **52**: 498–503
67 Taylor JP, Tanaka F, Robitschek J, Sandoval CM, Taye A, Markovic-Plese S, Fischbeck KH. Aggresomes protect cells by enhancing the degradation of toxic polyglutamine-containing protein. *Hum Mol Genet* 2003; **12**: 749–57
68 Ravikumar B, Duden R, Rubinsztein DC. Aggregate-prone proteins with polyglutamine and polyalanine expansions are degraded by autophagy. *Hum Mol Genet* 2002; **11**: 1107–17
69 Kegel KB, Kim M, Sapp E, McIntyre C, Castano JG, Aronin N, DiFiglia M. Huntingtin expression stimulates endosomal-lysosomal activity, endosome tubulation, and autophagy. *J Neurosci* 2000; **20**: 7268–78
70 Ishisaka R, Utsumi T, Yabuki M, Kanno T, Furuno T, Inoue M, Utsumi K. Activation of caspase-3-like protease by digitonin-treated lysosomes. *FEBS Lett* 1998; **435**: 233–6
71 Gatchel JR, Zoghbi HY. Diseases of unstable repeat expansion: mechanisms and common principles. *Nat Rev Genet* 2005; **6**: 743–55
72 Yeh S, Tsai MY, Xu Q, Mu XM, Lardy H, Huang KE, Lin H, Yeh SD, Altuwaijri S, Zhou X, Xing L, Boyce BF, Hung MC, Zhang S, Gan L, Chang C. Generation and characterization of androgen receptor knockout (ARKO) mice: an in vivo model for the study of androgen functions in selective tissues. *Proc Natl Acad Sci USA* 2002; **99**: 13498–503
73 Adachi H, Kume A, Li M, Nakagomi Y, Niwa H, Do J, Sang C, Kobayashi Y, Doyu M, Sobue G. Transgenic mice with an expanded CAG repeat controlled by the human AR promoter show polyglutamine nuclear inclusions and neuronal dysfunction without neuronal cell death. *Hum Mol Genet* 2001; **10**: 1039–48
74 Yu Z, Dadgar N, Albertelli M, Scheller A, Albin RL, Robins DM, Lieberman AP. Abnormalities of germ cell maturation and sertoli cell cytoskeleton in androgen receptor 113 CAG knock-in mice reveal toxic effects of the mutant protein. *Am J Pathol* 2006; **168**: 195–204
75 Thomas PS Jr, Fraley GS, Damien V, Woodke LB, Zapata F, Sopher BL, Plymate SR, La Spada AR. Loss of endogenous androgen receptor protein accelerates motor neuron degeneration and accentuates androgen insensitivity in a mouse model of X-linked spinal and bulbar muscular atrophy. *Hum Mol Genet* 2006; **15**: 2225–38
76 Kemppainen JA, Lane MV, Sar M, Wilson EM. Androgen receptor phosphorylation, turnover, nuclear transport, and transcriptional activation. Specificity for steroids and antihormones. *J Biol Chem* 1992; **267**: 968–74
77 Lieberman AP, Harmison G, Strand AD, Olson JM, Fischbeck KH. Altered transcriptional regulation in cells expressing the expanded polyglutamine androgen receptor. *Hum Mol Genet* 2002; **11**: 1967–76
78 Merry DE. Animal models of Kennedy disease. *Neurorx* 2005; **2**: 471–9
79 Chevalier-Larsen ES, O'Brien CJ, Wang H, Jenkins SC, Holder L, Lieberman AP, Merry DE. Castration restores

function and neurofilament alterations of aged symptomatic males in a transgenic mouse model of spinal and bulbar muscular atrophy. *J Neurosci* 2004; **24**: 4778–86

80 Banno H, Adachi H, Katsuno M, Suzuki K, Atsuta N, Watanabe H, Tanaka F, Doyu M, Sobue G. Mutant androgen receptor accumulation in spinal and bulbar muscular atrophy scrotal skin: a pathogenic marker. *Ann Neurol* 2006; **59**: 520–6

81 Fang Y, Fliss AE, Robins DM, Caplan AJ. Hsp90 regulates androgen receptor hormone binding affinity in vivo. *J Biol Chem* 1996; **271**: 28697–702

82 Georget V, Terouanne B, Nicolas JC, Sultan C. Mechanism of antiandrogen action: key role of hsp90 in conformational change and transcriptional activity of the androgen receptor. *Biochemistry* 2002; **41**: 11824–31

83 Pratt WB, Toft DO. Regulation of signaling protein function and trafficking by the hsp90/hsp70-based chaperone machinery. *Exp Biol Med (Maywood)* 2003; **228**: 111–33

84 Sullivan W, Stensgard B, Caucutt G, Bartha B, McMahon N, Alnemri ES, Litwack G, Toft D. Nucleotides and two functional states of hsp90. *J Biol Chem* 1997; **272**: 8007–12

85 Neckers L. Heat shock protein 90 inhibition by 17-allylamino-17-demethoxygeldanamycin: a novel therapeutic approach for treating hormone-refractory prostate cancer. *Clin Cancer Res* 2002; **8**: 962–6

86 Egorin MJ, Zuhowski EG, Rosen DM, Sentz DL, Covey JM, Eiseman JL. Plasma pharmacokinetics and tissue distribution of 17-(allylamino)-17-demethoxygeldanamycin (NSC 330507) in CD2F1 mice1. *Cancer Chemother Pharmacol* 2001; **47**: 291–302

87 McClellan AJ, Scott MD, Frydman J. Folding and quality control of the VHL tumor suppressor proceed through distinct chaperone pathways. *Cell* 2005; **121**: 739–48

88 Felts SJ, Toft DO. p23, a simple protein with complex activities. *Cell Stress Chaperones* 2003; **8**: 108–13

89 Mimnaugh EG, Chavany C, Neckers L. Polyubiquitination and proteasomal degradation of the p185c-erbB-2 receptor protein-tyrosine kinase induced by geldanamycin. *J Biol Chem* 1996; **271**: 22796–801

90 Bonvini P, Dalla Rosa H, Vignes N, Rosolen A. Ubiquitination and proteasomal degradation of nucleophosmin-anaplastic lymphoma kinase induced by 17-allylamino-demethoxygeldanamycin: role of the co-chaperone carboxyl heat shock protein 70-interacting protein. *Cancer Res* 2004; **64**: 3256–64

91 Smith DF, Whitesell L, Nair SC, Chen S, Prapapanich V, Rimerman RA. Progesterone receptor structure and function altered by geldanamycin, an hsp90-binding agent. *Mol Cell Biol* 1995; **15**: 6804–12

92 Johnson JL, Toft DO. Binding of p23 and hsp90 during assembly with the progesterone receptor. *Mol Endocrinol* 1995; **9**: 670–8

93 Vanaja DK, Mitchell SH, Toft DO, Young CY. Effect of geldanamycin on androgen receptor function and stability. *Cell Stress Chaperones* 2002; **7**: 55–64

94 Solit DB, Zheng FF, Drobnjak M, Munster PN, Higgins B, Verbel D, Heller G, Tong W, Cordon-Cardo C, Agus DB, Scher HI, Rosen N. 17-Allylamino-17-demethoxygeldanamycin induces the degradation of androgen receptor and HER-2/neu and inhibits the growth of prostate cancer xenografts. *Clin Cancer Res* 2002; **8**: 986–93

95 Neckers L. Hsp90 inhibitors as novel cancer chemotherapeutic agents. *Trends Mol Med* 2002; **8**: S55–61

96 Xiao N, Callaway CW, Lipinski CA, Hicks SD, DeFranco DB. Geldanamycin provides posttreatment protection against glutamate-induced oxidative toxicity in a mouse hippocampal cell line. *J Neurochem* 1999; **72**: 95–101

97 Sano M. Radicicol and geldanamycin prevent neurotoxic effects of anti-cancer drugs on cultured embryonic sensory neurons. *Neuropharmacology* 2001; **40**: 947–53

98 Xu L, Ouyang YB, Giffard RG. Geldanamycin reduces necrotic and apoptotic injury due to oxygen-glucose deprivation in astrocytes. *Neurol Res* 2003; **25**: 697–700

99 Ouyang YB, Xu L, Giffard RG. Geldanamycin treatment reduces delayed CA1 damage in mouse hippocampal organotypic cultures subjected to oxygen glucose deprivation. *Neurosci Lett* 2005; **380**: 229–33

100 Waza M, Adachi H, Katsuno M, Minamiyama M, Sang C, Tanaka F, Inukai A, Doyu M, Sobue G. 17-AAG, an Hsp90 inhibitor, ameliorates polyglutamine-mediated motor neuron degeneration. *Nat Med* 2005; **11**: 1088–95

101 Sittler A, Lurz R, Lueder G, Priller J, Lehrach H, Hayer-Hartl MK, Hartl FU, Wanker EE. Geldanamycin activates a heat shock response and inhibits huntingtin aggregation in a cell culture model of Huntington's disease. *Hum Mol Genet* 2001; **10**: 1307–15

102 Harrell JM, Murphy PJ, Morishima Y, Chen H, Mansfield JF, Galigniana MD, Pratt WB. Evidence for glucocorticoid receptor transport on microtubules by dynein. *J Biol Chem* 2004; **279**: 54647–54

103 Wochnik GM, Ruegg J, Abel GA, Schmidt U, Holsboer F, Rein T. FK506-binding proteins 51 and 52 differentially regulate dynein interaction and nuclear translocation of the glucocorticoid receptor in mammalian cells. *J Biol Chem* 2005; **280**: 4609–16

104 Thomas M, Harrell JM, Morishima Y, Peng HM, Pratt WB, Lieberman AP. Pharmacologic and genetic inhibition of hsp90-dependent trafficking reduces aggregation and promotes degradation of the expanded glutamine androgen receptor without stress protein induction. *Hum Mol Genet* 2006; **15**: 1876–83

105 Adachi H, Katsuno M, Minamiyama M, Sang C, Pagoulatos G, Angelidis C, Kusakabe M, Yoshiki A, Kobayashi Y, Doyu M, Sobue G. Heat shock protein 70 chaperone

overexpression ameliorates phenotypes of the spinal and bulbar muscular atrophy transgenic mouse model by reducing nuclear-localized mutant androgen receptor protein. *J Neurosci* 2003; **23**: 2203–11
106 Minamiyama M, Katsuno M, Adachi H, Waza M, Sang C, Kobayashi Y, Tanaka F, Doyu M, Inukai A, Sobue G. Sodium butyrate ameliorates phenotypic expression in a transgenic mouse model of spinal and bulbar muscular atrophy. *Hum Mol Genet* 2004; **13**: 1183–92
107 Whitesell L, Bagatell R, Falsey R. The stress response: implications for the clinical development of hsp90 inhibitors. *Curr Cancer Drug Targets* 2003; **3**: 349–58
108 Kamal A, Boehm MF, Burrows FJ. Therapeutic and diagnostic implications of Hsp90 activation. *Trends Mol Med* 2004; **10**: 283–90
109 Muchowski PJ, Wacker JL. Modulation of neurodegeneration by molecular chaperones. *Nat Rev Neurosci* 2005; **6**: 11–22
110 Xia H, Mao Q, Eliason SL, Harper SQ, Martins IH, Orr HT, Paulson HL, Yang L, Kotin RM, Davidson BL. RNAi suppresses polyglutamine-induced neurodegeneration in a model of spinocerebellar ataxia. *Nat Med* 2004; **10**: 816–20
111 Harper SQ, Staber PD, He X, Eliason SL, Martins IH, Mao Q, Yang L, Kotin RM, Paulson HL, Davidson BL. RNA interference improves motor and neuropathological abnormalities in a Huntington's disease mouse model. *Proc Natl Acad Sci USA* 2005; **102**: 5820–5
112 Raoul C, Abbas-Terki T, Bensadoun JC, Guillot S, Haase G, Szulc J, Henderson CE, Aebischer P. Lentiviral-mediated silencing of SOD1 through RNA interference retards disease onset and progression in a mouse model of ALS. *Nat Med* 2005; **11**: 423–8
113 La Spada AR, Weydt P. Targeting toxic proteins for turnover. *Nat Med* 2005; **11**: 1052–3
114 Cummings CJ, Mancini MA, Antalffy B, DeFranco DB, Orr HT, Zoghbi HY. Chaperone suppression of aggregation and altered subcellular proteasome localization imply protein misfolding in SCA1. *Nat Genet* 1998; **19**: 148–54
115 Ciechanover A, Brundin P. The ubiquitin proteasome system in neurodegenerative diseases: sometimes the chicken, sometimes the egg. *Neuron* 2003; **40**: 427–46
116 Bence NF, Sampat RM, Kopito RR. Impairment of the ubiquitin-proteasome system by protein aggregation. *Science* 2001; **292**: 1552–5
117 Jana NR, Zemskov EA, Wang G, Nukina N. Altered proteasomal function due to the expression of polyglutamine-expanded truncated N-terminal huntingtin induces apoptosis by caspase activation through mitochondrial cytochrome c release. *Hum Mol Genet* 2001; **10**: 1049–59
118 Holmberg CI, Staniszewski KE, Mensah KN, Matouschek A, Morimoto RI. Inefficient degradation of truncated polyglutamine proteins by the proteasome. *EMBO J* 2004; **23**: 4307–18
119 Zhou H, Cao F, Wang Z, Yu ZX, Nguyen HP, Evans J, Li SH, Li XJ. Huntingtin forms toxic NH2-terminal fragment complexes that are promoted by the age-dependent decrease in proteasome activity. *J Cell Biol* 2003; **163**: 109–18
120 Bett JS, Goellner GM, Woodman B, Pratt G, Rechsteiner M, Bates GP. Proteasome impairment does not contribute to pathogenesis in R6/2 Huntington's disease mice: exclusion of proteasome activator REG{gamma} as a therapeutic target. *Hum Mol Genet* 2006; **15**: 33–44
121 Yamamoto A, Lucas JJ, Hen R. Reversal of neuropathology and motor dysfunction in a conditional model of Huntington's disease. *Cell* 2000; **101**: 57–66
122 Zu T, Duvick LA, Kaytor MD, Berlinger MS, Zoghbi HY, Clark HB, Orr HT. Recovery from polyglutamine-induced neurodegeneration in conditional SCA1 transgenic mice. *J Neurosci* 2004; **24**: 8853–61
123 Macario AJ, Conway de Macario E. Sick chaperones, cellular stress, and disease. *N Engl J Med* 2005; **353**: 1489–501
124 Heinlein CA, Chang C. Role of chaperones in nuclear translocation and transactivation of steroid receptors. *Endocrine* 2001; **14**: 143–9
125 Rokutan K, Hirakawa T, Teshima S, Nakano Y, Miyoshi M, Kawai T, Konda E, Morinaga H, Nikawa T, Kishi K. Implications of heat shock/stress proteins for medicine and disease. *J Med Invest* 1998; **44**: 137–47
126 Warrick JM, Chan HY, Gray-Board GL, Chai Y, Paulson HL, Bonini NM. Suppression of polyglutamine-mediated neurodegeneration in Drosophila by the molecular chaperone HSP70. *Nat Genet* 1999; **23**: 425–8
127 Wyttenbach A, Carmichael J, Swartz J, Furlong RA, Narain Y, Rankin J, Rubinsztein DC. Effects of heat shock, heat shock protein 40 (HDJ-2), and proteasome inhibition on protein aggregation in cellular models of Huntington's disease. *Proc Natl Acad Sci USA* 2000; **97**: 2898–903
128 Wyttenbach A. Role of heat shock proteins during polyglutamine neurodegeneration: mechanisms and hypothesis. *J Mol Neurosci* 2004; **23**: 69–96
129 Kobayashi Y, Kume A, Li M, Doyu M, Hata M, Ohtsuka K, Sobue G. Chaperones Hsp70 and Hsp40 suppress aggregate formation and apoptosis in cultured neuronal cells expressing truncated androgen receptor protein with expanded polyglutamine tract. *J Biol Chem* 2000; **275**: 8772–8
130 Bailey CK, Andriola IF, Kampinga HH, Merry DE. Molecular chaperones enhance the degradation of expanded polyglutamine repeat androgen receptor in a cellular model of spinal and bulbar muscular atrophy. *Hum Mol Genet* 2002; **11**: 515–23
131 Cummings CJ, Sun Y, Opal P, Antalffy B, Mestril R, Orr HT, Dillmann WH, Zoghbi HY. Over-expression of inducible HSP70 chaperone suppresses neuropathology and improves motor function in SCA1 mice. *Hum Mol Genet* 2001; **10**: 1511–18

132 Hay DG, Sathasivam K, Tobaben S, Stahl B, Marber M, Mestril R, Mahal A, Smith DL, Woodman B, Bates GP. Progressive decrease in chaperone protein levels in a mouse model of Huntington's disease and induction of stress proteins as a therapeutic approach. *Hum Mol Genet* 2004; **13**: 1389–405

133 Agrawal N, Pallos J, Slepko N, Apostol BL, Bodai L, Chang LW, Chiang AS, Thompson LM, Marsh JL. Identification of combinatorial drug regimens for treatment of Huntington's disease using Drosophila. *Proc Natl Acad Sci USA* 2005; **102**: 3777–81

134 Dou F, Netzer WJ, Tanemura K, Li F, Hartl FU, Takashima A, Gouras GK, Greengard P, Xu H. Chaperones increase association of tau protein with microtubules. *Proc Natl Acad Sci USA* 2003; **100**: 721–6

135 Petrucelli L, Dickson D, Kehoe K, Taylor J, Snyder H, Grover A, De Lucia M, McGowan E, Lewis J, Prihar G, Kim J, Dillmann WH, Browne SE, Hall A, Voellmy R, Tsuboi Y, Dawson TM, Wolozin B, Hardy J, Hutton M. CHIP and Hsp70 regulate tau ubiquitination, degradation and aggregation. *Hum Mol Genet* 2004; **13**: 703–14

136 Benussi L, Ghidoni R, Paterlini A, Nicosia F, Alberici AC, Signorini S, Barbiero L, Binetti G. Interaction between tau and alpha-synuclein proteins is impaired in the presence of P301L tau mutation. *Exp Cell Res* 2005; **308**: 78–84

137 Auluck PK, Bonini NM. Pharmacological prevention of Parkinson disease in Drosophila. *Nat Med* 2002; **8**: 1185–6

138 Auluck PK, Meulener MC, Bonini NM. Mechanisms of suppression of {alpha}-synuclein neurotoxicity by geldanamycin in Drosophila. *J Biol Chem* 2005; **280**: 2873–8

139 Flower TR, Chesnokova LS, Froelich CA, Dixon C, Witt SN. Heat shock prevents alpha-synuclein-induced apoptosis in a yeast model of Parkinson's disease. *J Mol Biol* 2005; **351**: 1081–100

140 Lu A, Ran R, Parmentier-Batteur S, Nee A, Sharp FR. Geldanamycin induces heat shock proteins in brain and protects against focal cerebral ischemia. *J Neurochem* 2002; **81**: 355–64

141 Giffard RG, Xu L, Zhao H, Carrico W, Ouyang Y, Qiao Y, Sapolsky R, Steinberg G, Hu B, Yenari MA. Chaperones, protein aggregation, and brain protection from hypoxic/ischemic injury. *J Exp Biol* 2004; **207**: 3213–20

142 Murphy P, Sharp A, Shin J, Gavrilyuk V, Dello Russo C, Weinberg G, Sharp FR, Lu A, Heneka MT, Feinstein DL. Suppressive effects of ansamycins on inducible nitric oxide synthase expression and the development of experimental autoimmune encephalomyelitis. *J Neurosci Res* 2002; **67**: 461–70

143 Hirakawa T, Rokutan K, Nikawa T, Kishi K. Geranylgeranylacetone induces heat shock proteins in cultured guinea pig gastric mucosal cells and rat gastric mucosa. *Gastroenterology* 1996; **111**: 345–57

144 Katsuno M, Sang C, Adachi H, Minamiyama M, Waza M, Tanaka F, Doyu M, Sobue G. Pharmacological induction of heat-shock proteins alleviates polyglutamine-mediated motor neuron disease. *Proc Natl Acad Sci USA* 2005; **102**: 16801–6

145 Cowan KJ, Diamond MI, Welch WJ. Polyglutamine protein aggregation and toxicity are linked to the cellular stress response. *Hum Mol Genet* 2003; **12**: 1377–91

146 Batulan Z, Shinder GA, Minotti S, He BP, Doroudchi MM, Nalbantoglu J, Strong MJ, Durham HD. High threshold for induction of the stress response in motor neurons is associated with failure to activate HSF1. *J Neurosci* 2003; **23**: 5789–98

Received 29 August 2006
Accepted after revision 18 December 2006

Usefulness of combined fractional anisotropy and apparent diffusion coefficient values for detection of involvement in multiple system atrophy

Mizuki Ito, Hirohisa Watanabe, Yoshinari Kawai, Naoki Atsuta, Fumiaki Tanaka, Shinji Naganawa, Hiroshi Fukatsu and Gen Sobue

J. Neurol. Neurosurg. Psychiatry 2007;78;722-728; originally published online 12 Mar 2007;
doi:10.1136/jnnp.2006.104075

PAPER

Usefulness of combined fractional anisotropy and apparent diffusion coefficient values for detection of involvement in multiple system atrophy

Mizuki Ito, Hirohisa Watanabe, Yoshinari Kawai, Naoki Atsuta, Fumiaki Tanaka, Shinji Naganawa, Hiroshi Fukatsu, Gen Sobue

J Neurol Neurosurg Psychiatry 2007;**78**:722–728. doi: 10.1136/jnnp.2006.104075

See end of article for authors' affiliations

Correspondence to: Professor Gen Sobue, Department of Neurology, Nagoya University Graduate School of Medicine, 65 Tsurumai-cho Showa-ku, Nagoya 466-8550, Japan; sobueg@med.nagoya-u.ac.jp

Received 8 August 2006
Revised 12 February 2007
Accepted 4 March 2007
Published Online First 12 March 2007

Objective: To determine whether apparent diffusion coefficient (ADC) values and fractional anisotropy (FA) values can detect early pathological involvement in multiple system atrophy (MSA), and be used to differentiate MSA-P (multiple system atrophy if parkinsonian features predominate) from Parkinson's disease (PD).

Methods: We compared ADC and FA values in the pons, cerebellum and putamen of 61 subjects (20 probable MSA patients, 21 age matched PD patients and 20 age matched healthy controls) using a 3.0 T magnetic resonance system.

Results: ADC values in the pons, cerebellum and putamen were significantly higher, and FA values lower in MSA than in PD or controls. These differences were prominent in MSA lacking dorsolateral putaminal hyperintensity (DPH) or hot cross bun (HCB) sign. In differentiating MSA-P from PD using FA and ADC values, we obtained equal sensitivity (70%) and higher specificity (100%) in the pons than in the putamen and cerebellum. In addition, all patients that had both significant low FA and high ADC values in each of these three areas were MSA-P cases, and those that had both normal FA and ADC values in the pons were all PD cases. Our diagnostic algorithm based on these results accurately diagnosed 90% of patients with MSA-P.

Conclusion: FA and ADC values detected early pathological involvement prior to magnetic resonance signal changes in MSA. In particular, low FA values in the pons showed high specificity in discriminating MSA-P from PD. In addition, combined analysis of both FA and ADC values in all three areas was more useful than only one.

Multiple system atrophy (MSA) is a sporadic adult onset neurodegenerative disease presenting a combination of parkinsonism, cerebellar ataxia and autonomic failure during the course of the illness.[1–4] A consensus statement recommended designating patients as having MSA-P if parkinsonian features predominated or MSA-C if cerebellar features predominated.[5] Differentiation of Parkinson's disease (PD) from MSA-P is particularly important because these disorders differ in progression, prognosis and treatment responses.[6] However, a purely clinical differentiation, especially in the early phase of the disease, remains challenging.

In advanced MSA, MRI reliably shows characteristic signal changes, such as dorsolateral putaminal hyperintensity (DPH) and the hot cross bun (HCB) sign,[7–10] but these signs are not useful for differentiation between MSA-P and PD in their early phases.[11]

Apparent diffusion coefficient (ADC) values and fractional anisotropy (FA) values are new parameters on MRI, and these were used to evaluate the degree of tissue degeneration in various disorders. ADC values measure the average water diffusion, and increasing ADC values indicate tissue degeneration. FA values measure the degree of anisotropy of the diffusing water along different axes of the image, and decreasing FA values represent tissue degeneration. Recently, there have been some reports concerning ADC and FA values in MSA-P and PD patients. ADC values in the striatum were higher in MSA-P than in PD,[12] and those in the basis pontis and cerebellum were higher in MSA-C than in controls.[13] FA values in the middle cerebellar penduncle, basis pontis and internal capsule were lower in MSA-C than in controls.[14] However, these results still do not confirm whether ADC and FA values are really effective at discriminating MSA-P from PD, particularly in their early phases. To confirm the hypothesis that ADC and FA values can detect abnormalities in patients with MSA, even without DPH and HCB, and discriminate MSA-P from PD, a direct study of these values at various stages of MSA and PD and in various regions is needed.

The aim of the present investigation was to examine the utility of ADC and FA values in the pons, cerebellum and putamen to detect not only the early pathological changes in MSA but also to differentiate MSA-P from PD.

PATIENTS AND METHODS

We studied 61 subjects (20 consecutive patients with probable MSA (10 MSA-C; 10 MSA-P), 21 age and sex matched patients with probable PD and 20 age and sex matched healthy volunteers) (table 1). There was a significant difference in the duration from initial symptoms to MRI evaluation between MSA (4 (2) years, range 1–10) and PD (10 (8) years, range 1–30) patients. Furthermore, patients with MSA-P and PD were assessed using the Hohen–Yahr score. There was no significant difference in the Hohen–Yahr score between the MSA-P (3.6 (1.0)) and PD (3.5 (1.0)) groups. Patients in the relatively early stage of MSA were included in this study. Clinical diagnoses of MSA[5] and PD[15] were established by consensus diagnostic

Abbreviations: ADC, apparent diffusion coefficient; DPH, dorsolateral putaminal hyperintensity; FA, fractional anisotropy; HCB, hot cross bun; MSA, multiple system atrophy; MSA-C, multiple system atrophy if cerebellar features predominate; MSA-P, multiple system atrophy if parkinsonian features predominate; PD, Parkinson's disease; ROC, receiver operating characteristic; ROI, region of interest

Table 1 Patients data

	No of cases	Age (y)	Sex (F/M)	Duration (y)	H–Y
MSA	20	61 (9)	8/12	4 (2)	
MSA-P	10	63 (11)	4/6	4 (3)	3.6 (1.0)
MSA-C	10	58 (7)	4/6	4 (2)	
PD	21	62 (11)	13/8	10 (8)	3.5 (1.0)
Control	20	62 (11)	13/7		

ADC, apparent diffusion coefficient; DPH, dorsolateral putaminal hyperintensity; FA, fractional anisotropy; HCB, hot cross bun; MSA, multiple system atrophy; MSA-C, multiple system atrophy if cerebellar features predominate; MSA-P, multiple system atrophy if parkinsonian features predominate; PD, Parkinson's disease.

criteria. All MSA patients fulfilled clinically probable criteria. In addition, controls underwent the same MRI examination. Informed consent was established before subject participation. This study was approved by the ethics committee of the Nagoya University Graduate School of Medicine.

MRI protocol

All scanning was carried out with a 3.0 T MR scanner (Trio, Siemens, Erlangen, Germany), using a receive only 8 channel phased array head coil. Diffusion weighted imaging was obtained with optimal methods[16] using a Stejskal–Tanner sequence with single shot spin echo-type echo planar imaging, flip angle of 90° and a repetition time of 7700 ms. Echo times corresponding to respective b-factors were 75 ms for 700 s/mm^2. Echo spacing was 0.79 ms, and matrix size was 128×128 with a readout bandwidth of 1562 Hz/pixel. Sixty axial slices, 2 mm thick with a 0.6 mm interslice gap, were used to image the entire brain with a 23 cm square field of view.

A motion probing gradient was applied in six orientations after acquisition of b = 700 images. The 128×128 data matrix was zero fill interpolated to 256×256. An acceleration factor of 2 was applied using the parallel imaging technique, generalised autocalibrating partially parallel acquisitions (GRAPPA),[17] which is an extension of the simultaneous acquisition of spatial harmonics technique. Eddy current related geometric distortions were not prominent between the images of each motion probing gradient directions and thus distortion correction post-processing was not applied.

Data analyses

ADC and FA values, and tractography were obtained using the public domain software dTV II for diffusion weighted imaging analysis developed by the Imaging Computing and Analysis Laboratory (Department of Radiology, University of Tokyo Hospital, Japan), and made available via the URL http://www.ut-radiology.umin.jp/people/masutani/dTV.htm. Regions of interest (ROIs) in the pons and cerebellum were placed within closed curves drawn around the entire axially imaged pons and around the axial cerebellum section that showed the largest dentate nucleus profile (fig 1A, 1B). As it was difficult to discriminate the entire axial putamen on MRI, ROIs in the putamen were placed within closed fixed circles drawn on the axial putaminal section (fig 1C). Regional ADC and FA values were calculated in each ROI. Mean ADC and FA values were adapted as representative indices of ADC and FA values. For tractography visualisation in the pons and cerebellum, which could be anatomically analysed in their entirety, seed areas were defined on T2 weighted axial images (b = 0) as the interior of the previously mentioned closed curve drawn around the pons and cerebellum. The presence or absence of HCB or DPH signs[18] was determined on T2 weighted axial images of the pons or putamen by the radiologist.

Statistical analyses were performed using SPSS 11.0 for Windows (SPSS Inc, USA). The Kruskal–Wallis test was used for comparison of ADC or FA values among MSA, PD and controls or MSA-P, PD and controls. The significance level was set at $p<0.05$. In addition, to differentiate probable MSA-P from PD, we performed receiver operating characteristic (ROC) analysis for FA and ADC values in each ROI. Based on these ROC data, we set cut off points for FA and ADC values, respectively.

RESULTS

Features of tractography

Tractography in representative MSA, PD and control subjects is shown in fig 2. Compared with PD and controls, MSA showed a decreased volume of fibre bundles corresponding anatomically to the middle cerebellar peduncle, transverse pontine and pyramidal tract fibres located in the pontine ROI, and also to the middle cerebellar peduncle and frontocerebellar tract located in the cerebellar ROI. No marked difference was seen between PD and controls. Although these fibre bundle losses were prominent in most MSA patients, some MSA cases had relatively well preserved tractography.

FA and ADC values in the pons, cerebellum and putamen

FA values in the pons, cerebellum and putamen in MSA were significantly lower than those in PD or controls. With respect to MSA phenotype, FA values in all three areas were significantly lower in MSA-P and MSA-C than in either PD or controls (fig 3A–C). However, FA values in the pons and cerebellum tended to be lower in MSA-C than in MSA-P, but the differences were not significant. FA values in the putamen were similar in MSA-C and MSA-P subjects.

ADC values in the pons, cerebellum and putamen were significantly higher in MSA than in PD or controls. With respect to MSA phenotype, ADC values in all three areas were significantly higher in MSA-P or MSA-C than in PD or controls (fig 4A–C), while ADC values in the pons and cerebellum tended to be higher in MSA-C than in MSA-P, but the

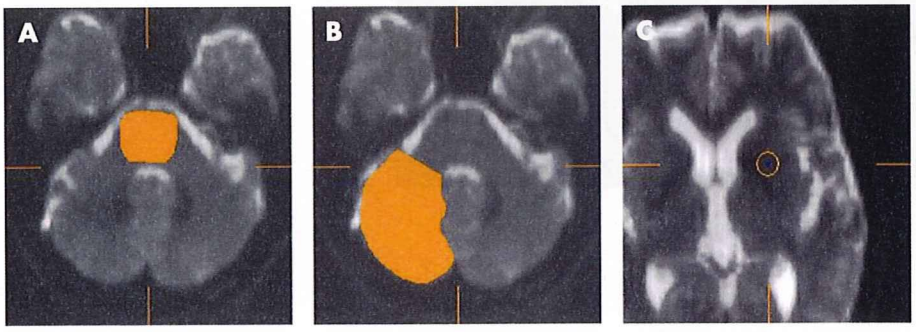

Figure 1 Regions of interest (ROI). ROIs in the pons (A), cerebellum (B) and putamen (C).

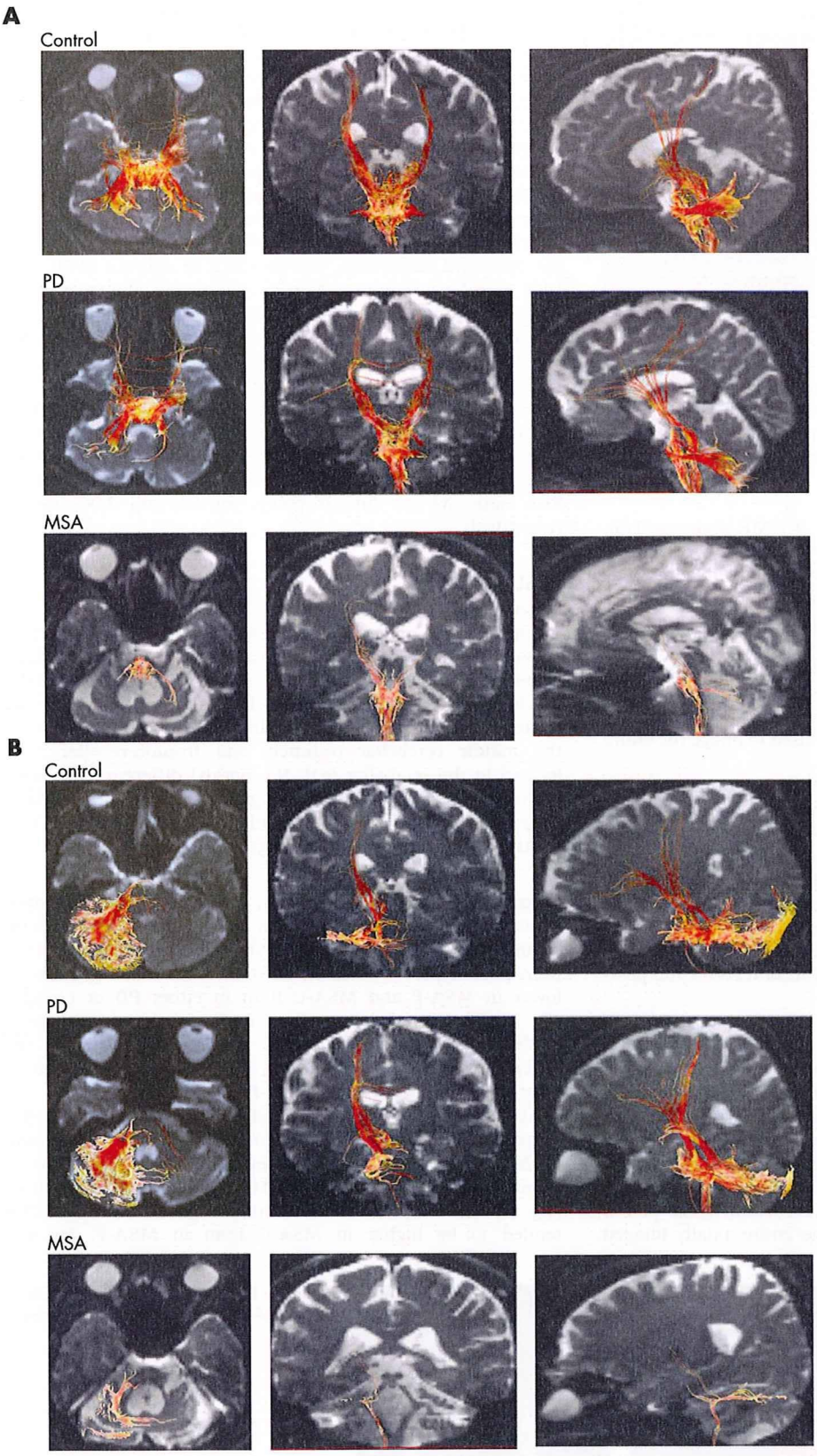

Figure 2 Tractography in the pons and cerebellum. (A) Pons. Visualisation of fibres in the pons and pyramidal tract fibres is unclear in multiple system atrophy (MSA). (B) Cerebellum. Visualisation of transverse fibres proceeding via the middle cerebellar peduncle, and of fibres connecting to the frontal lobe is unclear in MSA. PD, Parkinson's disease.

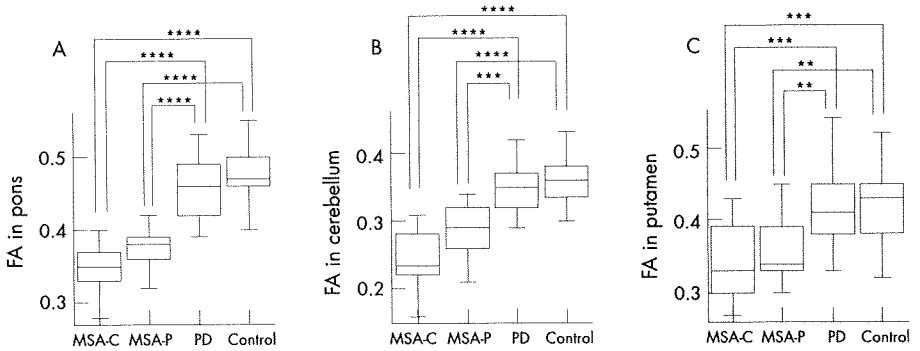

Figure 3 Fractional anisotropy (FA) values in the pons, cerebellum and putamen. FA values in multiple system atrophy if cerebellar features predominate (MSA-C), multiple system atrophy if parkinsonian features predominate (MSA-P), Parkinson's disease (PD) and controls are shown in the pons (A), cerebellum (B) and putamen (C). $^{**}p<0.01$, $^{***}p<0.005$, $^{****}p<0.001$. FA values in all three areas were significantly lower in MSA-P and MSA-C than in PD or controls.

difference was not significant. ADC values in the putamen were similar in MSA-C and MSA-P.

Statistically lower FA and higher ADC values in the pons and cerebellum were more prominent than those in the putamen.

FA and ADC values in MSA with or without magnetic resonance signal changes

In our MSA patients, specificity of the HCB and DPH signs were both 100%, while sensitivity of the HCB and DPH signs were only 45.0% and 40.0%, respectively. However, in 11 MSA patients without the HCB sign, 8 (72.7%) showed low FA values in the pons, 7 (63.6%) in the cerebellum and 6 (54.5%) in the putamen, and 8 (72.7%) showed high ADC values in the pons, 6 (54.5%) in the cerebellum and 8 (72.7%) in the putamen (table 2). In 12 MSA patients without the DPH sign, 10 (83.3%) showed low FA values in the pons, 10 (83.3%) in the cerebellum and 10 (83.3%) in the putamen, and 8 (66.7%) showed high ADC values in the pons, 9 (75.0%) in the cerebellum and 6 (50.0%) in the putamen (table 2). These observations demonstrate that changes in FA and ADC values can be detected prior to the appearance of HCB and DPH signs in early phase MSA. FA values were significantly lower in MSA patients without DPH or HCB signs than in PD patients. Likewise, ADC values were significantly higher in MSA patients without DPH or HCB signs than in PD patients.

Differentiating MSA-P from PD

To differentiate probable MSA-P from PD, we performed ROC analysis. Based on these ROC data, we set cut off points for FA values in the pons, cerebellum and putamen at 0.38, 0.30 and 0.35, and for ADC values 0.98, 0.96 and 0.83, respectively, and that both sensitivity and specificity were as high as possible in our cases. Sensitivity and specificity based on these cut off points for FA values were 70.0% and 100.0% in the pons, 70.0% and 63.6% in the cerebellum and 70.0% and 87.5% in the putamen (fig 5). Sensitivity and specificity based on these cut off points for ADC values were 70.0% and 70.0% in the pons, 60.0% and 87.5% in the cerebellum and 70.0% and 63.6% in the putamen (fig 5). FA values in the pons were particularly useful for readily differentiating MSA-P from PD, and provided equal sensitivity and higher specificity than those in the cerebellum and putamen. Hence pontine FA values were especially useful markers to diagnose MSA-P as well as those in the cerebellum and putamen.

In addition, our results showed that three MSA-P patients had low FA but normal ADC values (fig 5A, red area) and three had normal FA but high ADC values (fig 5A, blue area) in the pons. In the cerebellum and putamen (fig 5B, C), two and two MSA-P patients, respectively, had low FA but normal ADC values, and one and two, respectively, had normal FA but high ADC values.

All patients that had both low FA and high ADC values in each of the three areas were probable MSA-P cases (fig 5A–C, purple areas), suggesting that patients with such values have a high possibility of being correctly diagnosed as MSA-P. Furthermore, no MSA cases had both normal FA and ADC values in the pons (fig 5A, white area), and all patients that had both normal FA and ADC values in the pons were PD cases. However, in the cerebellum and putamen (fig 5B, C, white areas), two and one MSA-P cases, respectively, had both normal FA and ADC values. Hence it was more useful to examine both FA and ADC values than only one or the other to distinguish MSA-P from PD.

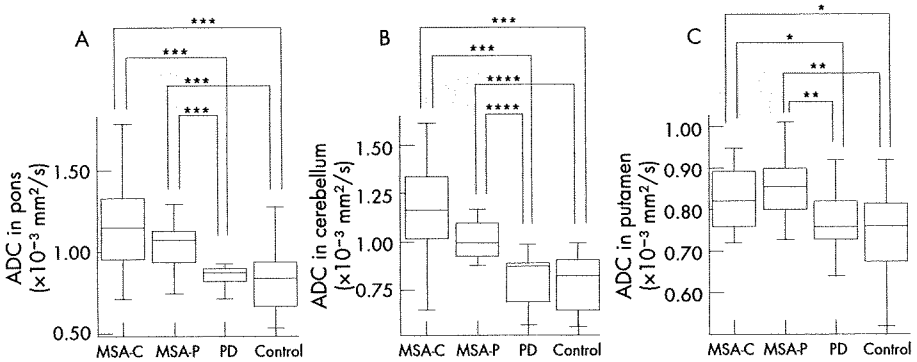

Figure 4 Apparent diffusion coefficient (ADC) values in the pons, cerebellum and putamen. ADC values ($\times 10^{-3}$ mm^2/s) in multiple system atrophy if cerebellar features predominate (MSA-C), multiple system atrophy if parkinsonian features predominate (MSA-P), Parkinson's disease (PD) and controls are shown in the pons (A), cerebellum (B) and putamen (C). $^{*}p<0.05$, $^{**}p<0.01$, $^{***}p<0.005$, $^{****}p<0.001$. ADC values in all three areas were significantly higher in MSA-P or MSA-C than in PD or controls.

Table 2 Percentage of patients with multiple system atrophy presenting with low fractional anisotropy or high apparent diffusion coefficient values without dorsolateral putaminal hyperintensity or hot cross bun signs

ROI	Cut off points	MSA patients without DPH sign (n = 12)	MSA patients without HCB sign (n = 11)
Pons			
	FA ⩽0.38	10 (83.3%)	8 (72.7%)
	ADC ⩾0.98	8 (66.7%)	8 (72.7%)
Cerebellum			
	FA ⩽0.30	10 (83.3%)	7 (63.6%)
	ADC ⩾0.96	9 (75.0%)	6 (54.5%)
Putamen			
	FA ⩽0.35	10 (83.3%)	6 (54.5%)
	ADC ⩾0.83	6 (50.0%)	8 (72.7%)

ADC, apparent diffusion coefficient; DPH, dorsolateral putaminal hyperintensity; FA, fractional anisotropy; HCB, hot cross bun; MSA, multiple system atrophy; ROI, region of interest.

Therefore, based on these results, we devised an algorithm for differentiating probable MSA-P from PD (fig 6). Using this algorithm in our 31 cases (PD 21; probable MSA-P 10), all patients that had both normal FA and ADC values in all three areas were PD cases (12 PD cases). In addition, all patients that had both low FA and high ADC values in any of the three areas were probable MSA-P cases (9 probable MSA-P cases). Taken together, the "MSA area" included 90.0% of probable MSA-P cases and no PD cases, and the "PD area" included 57.1% of PD cases and no probable MSA-P cases.

DISCUSSION

To our knowledge, this is the first systematic study to demonstrate the usefulness of simultaneous assessment of ADC and FA values on multiple regions, including the pons, cerebellum and putamen in MSA, PD and controls. We showed that low FA and high ADC values in these regions were significant even in MSA cases without HCB or DPH signs, suggesting that FA and ADC assessment can be a potent

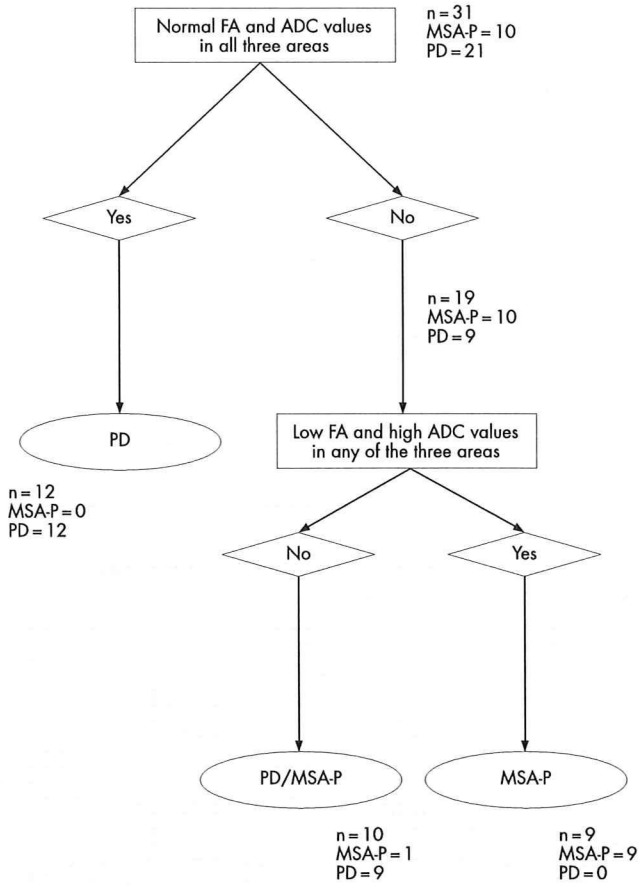

Figure 6 Algorithm for differentiating probable multiple system atrophy if parkinsonian features predominate (MSA-P) from Parkinson's disease (PD) using fractional anisotropy (FA) and apparent diffusion coefficient (ADC) values. Using this algorithm in our 31 cases (PD 21; probable MSA-P 10), the "MSA area" included 90% of probable MSA-P cases and no PD cases, and the "PD area" included 57.1% of PD cases and no MSA-P cases.

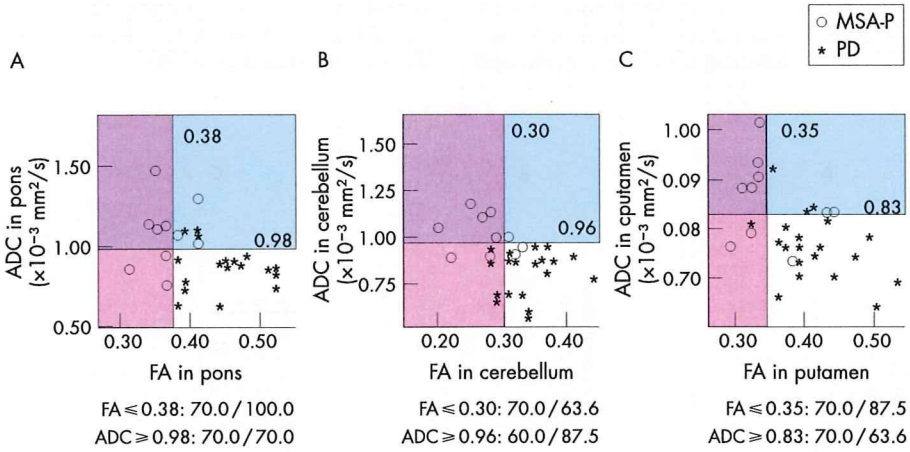

Figure 5 Differentiation of multiple system atrophy if parkinsonian features predominate (MSA-P) from Parkinson's disease (PD). Fractional anisotropy (FA) and apparent diffusion coefficient (ADC) values in the pons (A), cerebellum (B) and putamen (C). In the pons, cerebellum and putamen, the cut off point was set at 0.38, 0.30 and 0.35 for FA, and 0.98, 0.96 and 0.83 for ADC, respectively. Sensitivity/specificity in differentiating probable MSA-P from PD using these cut off points are shown. FA values in the pons were particularly useful for readily differentiating MSA-P from PD. In addition, some MSA-P cases had low FA and normal ADC values or normal FA and high ADC values. All patients that had both low FA and high ADC values in all three areas were MSA cases, and all patients that had both normal FA and ADC values in the pons were PD cases.

procedure to detect early involvement in MSA without diagnostic MRI findings. In particular, 90.0% of probable MSA-P cases showed a combination of low FA and high ADC values in one or more of the three areas, but no PD patients showed both low FA and high ADC values in any of the three areas. In addition, 57.1% of PD cases showed a combination of normal FA and ADC values in all three areas. These results suggest that combined evaluation of FA and ADC values in early disease stages provides an accurate method for differentiating MSA-P from PD.

ADC values measure the average water diffusion. High putaminal ADC values were reported to be helpful in differentiating MSA-P from PD.[12] Subsequently, brainstem ADC values in MSA-C were demonstrated to be increased.[13] As increases in ADC values have been shown in certain other diseases[19–21] and in normal aging,[22] high ADC values are thought to reflect destruction of tissue architecture. In contrast, FA values are new parameters specifically measuring the degree of anisotropy of the diffusing water along different axes of the image, enabling useful quantitative estimation of decreased tissue anisotropy reflecting degeneration. Reduced FA values have been reported in certain other diseases[23–25] and in normal aging.[26] More recently, decreased FA values in cerebellopetal fibres and pyramidal tracts have been reported in MSA-C,[14] and low FA values are also thought to reflect destruction of tissue architecture. In this study, we demonstrated that by using small voxels and optimised parameters,[16] as well as a generalised autocalibrating partially parallel acquisitions (GRAPPA)[17] algorithm for suppressing artefact and noise to obtain reliable ADC and FA values, as evidenced by clear tractography results, increased ADC and decreased FA values could reflect destruction of brainstem, cerebellar or putaminal tissue architecture resulting from neuronal loss and/or gliosis, enhancing random mobility of free water molecules within the tissue. Our results support previous observations and extend the significance of FA and ADC values in the diagnosis of MSA-P, even in cases without DPH or HCB signs.

Some of our MSA-P or PD cases showed a combination of normal FA but high ADC or low FA but normal ADC values in various regions. As above, high ADC and low FA values could reflect similar destruction of tissue architecture and have been demonstrated in various pathological changes, including brain atrophy, atherosclerotic change and normal aging.[22 26] However, these parameters are based on different pathological conditions. This may be one of the reasons why some cases showed normal FA but high ADC or low FA but normal ADC values. Furthermore, only cases of MSA-P had both low FA and high ADC values in each of the three areas. FA and ADC values may mutually provide additional information about the evolution of the disease that is not available from one method. These findings suggest that the combined evaluation of FA and ADC values could be more useful for early detection of pathological involvement in MSA-P than evaluation of either of these separately.

With respect to location, pontine FA and ADC values were especially useful markers in diagnosing MSA-P compared with those in the cerebellum and putamen. Although degeneration of olivopontocerebellar systems is evident from clinical features and MRI findings in MSA-C, these changes are not apparent in the early phase of MSA-P. The present study clearly demonstrated that even though reductions in FA values and increases in ADC values in the pons and cerebellum were more remarkable in MSA-C than in MSA-P, these changes were still highly evident in MSA-P. The question arises as to why significantly abnormal ADC and FA values can be seen in the pons even in early phase MSA. Patients with early stage MSA in Caucasian populations have been reported to show selective neuronal cell loss in the substantia nigra and locus coeruleus, with relative sparing of both the striatum and the olivopontocerebellar system.[27] One possible explanation may be that ADC and FA values have the potential to detect minimal and subclinical, but accumulated, neurodegeneration in the pons, because the pons contains the neurons and fibre tracts (eg, the pontine nuclei, transverse pontine fibres and corticospinal tracts) that are preferentially effected in MSA and thus could accumulate and reflect the MSA specific neurodegenerative process at an early phase of illness. Alternatively, it could be due to differences in the pathological features of MSA among Japanese and Caucasian populations. We previously reported that MSA-C was more frequent, and MSA-P less frequent, in Japanese populations[11] compared with Western populations,[3] and also that proton magnetic resonance spectroscopy (^{1}H-MRS) showed significantly lower N-acethylaspartate/creatine ratios in the basis pontis suggesting more neuroaxonal loss or dysfunction in MSA-P than in PD.[28] The olivopontocerebellar system shows more profound degeneration in Japanese MSA-P. While further study is needed to address this issue, we suggest that the pons is a beneficial region to detect early pathological change in MSA.

In previous reports,[12] ADC values in the dorsolateral putaminal ROIs were reported to be more useful in distinguishing MSA from PD compared with those in the anteroventral ROIs. It is interesting that this result corresponded well to the spatial distribution of pathological lesions in the putamen in MSA. In contrast, we used relatively large sized ROIs than previous reports to obtain reliable data under our MRI conditions, such as higher magnetic field strength, special software and parameters to analyse FA and ADC values. In addition, as some MSA and PD patients showed obscure putaminal edges on MRI, we set the ROIs in the relatively midst putamen, including dorsolateral parts. These specific MRI conditions may have caused the differences in the sensitivity and specificity in the putamen between our study and previous ones. These discrepancies may also be explained by ethnic differences. The olivopontocerebellar system could be more severely affected in Japanese than in Western populations. A multicentre survey will be needed to clarify the optimised size of ROIs, magnetic field strengths and parameters to standardise the FA and ADC values as diagnostic criteria.

In summary, combined evaluation of FA and ADC values in the putamen, cerebellum and putamen would provide useful information for highly and accurate differentiation of MSA-P from PD. Such early FA reduction and ADC increase are likely to be associated with subtle early degenerative processes in MSA, even without diagnostic magnetic resonance signal abnormalities. In addition, to justify our conclusion, it will be necessary to apply this algorithm, in a prospective manner, to patients with possible MSA without diagnostic MRI findings, and to determine whether these patients will develop full blown MSA symptoms in several years.

Authors' affiliations
Mizuki Ito, Hirohisa Watanabe, Yoshinari Kawai, Naoki Atsuta, Fumiaki Tanaka, Gen Sobue, Department of Neurology, Nagoya University Graduate School of Medicine, Nagoya, Japan
Shinji Naganawa, Hiroshi Fukatsu, Department of Radiology, Nagoya University Graduate School of Medicine, Nagoya, Japan

Competing interests: None.

REFERENCES

1 **Graham JG,** Oppenheimer DR. Orthostatic hypotension and nicotine sensitivity in a case of multiple system atrophy. *J Neurol Neurosurg Psychiatry* 1969;**32**:28–34.

2 **Quinn N**. Multiple system atrophy—the nature of the beast. *J Neurol Neurosurg Psychiatry* 1989;**52**:78–89.
3 **Wenning GK**, Tison F, Ben-Shlomo Y, *et al*. Multiple system atrophy: a review of 203 pathologically proven cases. *Mov Disord* 1997;**12**:133–47.
4 **Wenning GK**, Colosimo C, Geser F, *et al*. Multiple system atrophy. *Lancet Neurol* 2004;**3**:93–103.
5 **Gilman S**, Low PA, Quinn N, *et al*. Consensus statement on the diagnosis of multiple system atrophy. *J Neurol Sci* 1999;**163**:94–8.
6 **Wenning GK**, Ben-Shlomo Y, Hughes A, *et al*. What clinical features are most useful to distinguish definite multiple system atrophy from Parkinson's disease? *J Neurol Neurosurg Psychiatry* 2000;**68**:434–40.
7 **Savoiardo M**, Strada L, Girotti F, *et al*. Olivopontocerebellar atrophy: MR diagnosis and relationship to multiple system atrophy. *Radiology* 1990;**174**:693–6.
8 **Konagaya M**, Konagaya Y, Iida M. Clinical and magnetic resonance imaging study of extrapyramidal symptoms in multiple system atrophy. *J Neurol Neurosurg Psychiatry* 1994;**57**:1528–31.
9 **Schrag A**, Kingsley D, Phatouros C, *et al*. Clinical usefulness of magnetic resonance imaging in multiple system atrophy. *J Neurol Neurosurg Psychiatry* 1998;**65**:65–71.
10 **Kraft E**, Schwarz J, Trenkwalder C, *et al*. The combination of hypointense and hyperintense signal changes on T2-weighted magnetic resonance imaging sequences: a specific marker of multiple system atrophy? *Arch Neurol* 1999;**56**:225–8.
11 **Watanabe H**, Saito Y, Terao S, *et al*. Progression and prognosis in multiple system atrophy: an analysis of 230 Japanese patients. *Brain* 2002;**125**:1070–83.
12 **Schocke MF**, Seppi K, Esterhammer R, *et al*. Trace of diffusion tensor differentiates the Parkinson variant of multiple system atrophy and Parkinson's disease. *Neuroimage* 2004;**21**:1443–51.
13 **Kanazawa M**, Shimohata T, Terajima K, *et al*. Quantitative evaluation of brainstem involvement in mutiple system atrophy by diffusion-weighted MR imaging. *J Neurol* 2004;**251**:1121–4.
14 **Shiga K**, Yamada K, Yoshikawa K, *et al*. Local tissue anisotropy decreases in cerebellopetal fibers and pyramidal tract in multiple system atrophy. *J Neurol* 2005;**252**:589–96.
15 **Calne DB**, Snow BJ, Lee C. Criteria for diagnosing Parkinson's disease. *Ann Neurol* 1992;**32**:S125–7.
16 **Naganawa S**, Koshikawa T, Kawai H, *et al*. Optimization of diffusion-tensor MR imaging data acquisition parameters for brain fiber tracking using parallel imaging at 3T. *Eur Radiol* 2004;**14**:234–8.
17 **Griswold MA**, Jakob PM, Heidemann RM, *et al*. Generalized autocalibrating partially parallel acquisitions (GRAPPA). *Magn Reson Med* 2002;**47**:1202–10.
18 **Bhattacharya K**, Saadia D, Eisenkraft B, *et al*. Brain magnetic resonance imaging in multiple-system atrophy and Parkinson disease. *Arch Neurol* 2002;**59**:835–42.
19 **Schaefer PW**, Grant PE, Gonzalez RG. Diffusion-weighted MR imaging of the brain. *Radiology* 2000;**217**:331–45.
20 **Wilson M**, Morgan PS, Lin X, *et al*. Quantitative diffusion weighted magnetic resonance imaging, cerebral atrophy, and disability in multiple sclerosis. *J Neurol Neurosurg Psychiatry* 2001;**70**:318–22.
21 **Kantarci K**, Jack CR, Xu YC, *et al*. Mild cognitive impairment and Alzheimer disease: Regional diffusivity of water. *Radiology* 2001;**219**:101–7.
22 **Helenius J**, Soinne L, Perkio J, *et al*. Diffusion-weighted MR imaging in normal human brains in various age groups. *Am J Neuroradiol* 2002;**23**:194–9.
23 **Toosy AT**, Werring DJ, Orrell RW, *et al*. Diffusion tensor imaging detects corticospinal tract involvement at multiple levels in amyotrophic lateral sclerosis. *J Neurol Neurosurg Psychiatry* 2003;**74**:1250–7.
24 **Sugihara S**, Kinoshita T, Matsusue E, *et al*. Usefulness of diffusion tensor imaging of white matter in Alzheimer disease and vascular dementia. *Acta Radiol* 2004;**45**:658–63.
25 **Guo AC**, MacFall JR, Provenzale JM. Multiple sclerosis: diffusion tensor MR imaging for evaluation of normal appearing white matter. *Radiology* 2002;**222**:729–36.
26 **Abe O**, Aoki S, Hayashi N, *et al*. Normal aging in the central nervous system: quantitative MR diffusion-tensor analysis. *Neurobiol Aging* 2002;**23**:433–41.
27 **Wenning GK**, Quinn N, Magalhaes M, *et al*. "Minimal change" multiple system atrophy. *Mov Disord* 1994;**9**:161–6.
28 **Watanabe H**, Fukatsu H, Katsuno M, *et al*. Multiple regional 1H-MR spectroscopy in multiple system atrophy: NAA/Cr reduction in pontine base as a valuable diagnostic marker. *J Neurol Neurosurg Psychiatry* 2004;**75**:103–9.

nature medicine

ASC-J9 ameliorates spinal and bulbar muscular atrophy phenotype via degradation of androgen receptor

Zhiming Yang[1,2,7], Yu-Jia Chang[1,3,7], I-Chen Yu[1], Shuyuan Yeh[1], Cheng-Chia Wu[1,3], Hiroshi Miyamoto[1], Diane E Merry[4], Gen Sobue[5], Lu-Min Chen[1,6], Shu-Shi Chang[1,6] & Chawnshang Chang[1]

Motor neuron degeneration resulting from the aggregation of the androgen receptor with an expanded polyglutamine tract (AR-polyQ) has been linked to the development of spinal and bulbar muscular atrophy (SBMA or Kennedy disease). Here we report that adding 5-hydroxy-1,7-bis(3,4-dimethoxyphenyl)-1,4,6-heptatrien-3-one (ASC-J9) disrupts the interaction between AR and its coregulators, and also increases cell survival by decreasing AR-polyQ nuclear aggregation and increasing AR-polyQ degradation in cultured cells. Intraperitoneal injection of ASC-J9 into AR-polyQ transgenic SBMA mice markedly improved disease symptoms, as seen by a reduction in muscular atrophy. Notably, unlike previous approaches in which surgical or chemical castration was used to reduce SBMA symptoms, ASC-J9 treatment ameliorated SBMA symptoms by decreasing AR-97Q aggregation and increasing VEGF164 expression with little change of serum testosterone. Moreover, mice treated with ASC-J9 retained normal sexual function and fertility. Collectively, our results point to a better therapeutic and preventative approach to treating SBMA, by disrupting the interaction between AR and AR coregulators.

X-linked spinal and bulbar muscular atrophy (SBMA or Kennedy disease) is an inherited neurodegenerative disorder caused by the expansion of the polyglutamine tract of the androgen receptor (AR-polyQ)[1–3]. The length of the AR-polyQ tract is inversely correlated with the age of SBMA onset[1–3]. The effects of the disease are only seen in males, as female carriers are usually asymptomatic. Characteristics of SBMA include proximal muscular atrophy, weakness, contraction fasciculation and bulbar involvement[4]. The nuclear inclusions containing AR-polyQ in the residual motor neurons of the brain stem, spinal cord and other visceral organs[5] are considered to be relevant to the pathophysiology of this disease[6].

In normal individuals, AR (ref. 7), upon activation by androgen, functions as a transcriptional regulator[8] by interacting with a variety of coregulatory proteins[9,10]. In motor neurons, one of the key AR coregulators is the cAMP response element–binding protein (CREB)-binding protein (CBP)[11], which controls the expression of the gene encoding VEGF164 among other genes.

Several mechanisms have been proposed to explain the pathogenesis of SBMA and to suggest potential targets for medical intervention. These mechanisms, which are not necessarily mutually exclusive, include transcriptional deregulation[12], aggregate formation[11,13], proteolysis of causative proteins[14,15], transglutaminase activation[16] and mitochondrial deficits[17]. Transcriptional disturbance, for example through the sequestration of CBP by AR-polyQ aggregates, seems to be one of the most likely causes for the pathogenesis of SBMA. This notion is further supported by the fact that transcriptional deregulation occurs in polyQ-related diseases[18]. Consistent with this idea, manipulations such as chemical or surgical castration, which reduce the level of AR-97Q aggregates[19–21], as well as the administration of a histone deacetylase inhibitor, which restores CBP-mediated transcription, effectively treat SBMA in mice[20]. However, the severe side effects caused by castration, including loss of libido, impotence, osteoporosis and fatigue, and the toxicity of histone deacetylase inhibitors make these approaches unsuitable therapeutic strategies for treating SBMA in men.

A compound that disrupts aggregates comprised of AR-polyQ and various coregulators could have potential therapeutic benefits for two complementary reasons. First, such a compound could increase the level of transcriptionally active coregulators, including CBP, by releasing them from the nonproductive interaction with AR-polyQ. Second, disrupting the aggregates might render the released AR-polyQ more vulnerable to degradation, thereby reducing its toxic effect.

We screened natural products and their derivatives for the disruption of normal AR and its coregulators, and found that 5–hydroxy-1,7-bis(3,4-dimethoxyphenyl)-1,4,6-heptatrien-3-one (ASC-J9) can substantially promote the dissociation of AR and ARA70 (ref. 22). Moreover, we discovered that treatment of prostate cancer cells with ASC-J9 led to decreased AR transactivation, resulting in the suppression of AR-mediated cell proliferation[22]. Using a SBMA PC12/AR-112Q cell line[23] and a SBMA/AR-97Q line of transgenic mice[5] as models, we found that ASC-J9 ameliorated SBMA symptoms with little influence on the concentration of circulating testosterone.

[1]George Whipple Lab for Cancer Research, Departments of Pathology, Urology, and Radiation Oncology, and The Cancer Center, University of Rochester Medical Center, Rochester, New York 14642, USA. [2]Zhejiang University and 2nd Hospital, Hangzhou 310009, China. [3]Taipei Medical University and Hospital, Taipei 110, Taiwan. [4]Thomas Jefferson University, Philadelphia, Pennsylvania 19107, USA. [5]Nagoya University, Nagoya 466-8550, Japan. [6]China Medical University and Hospital, Taichung 404, Taiwan. [7]These authors contributed equally to this work. Correspondence should be addressed to C.C. (chang@URMC.rochester.edu).

Received 10 March 2006; accepted 16 January 2007; published online 4 March 2007; doi:10.1038/nm1547

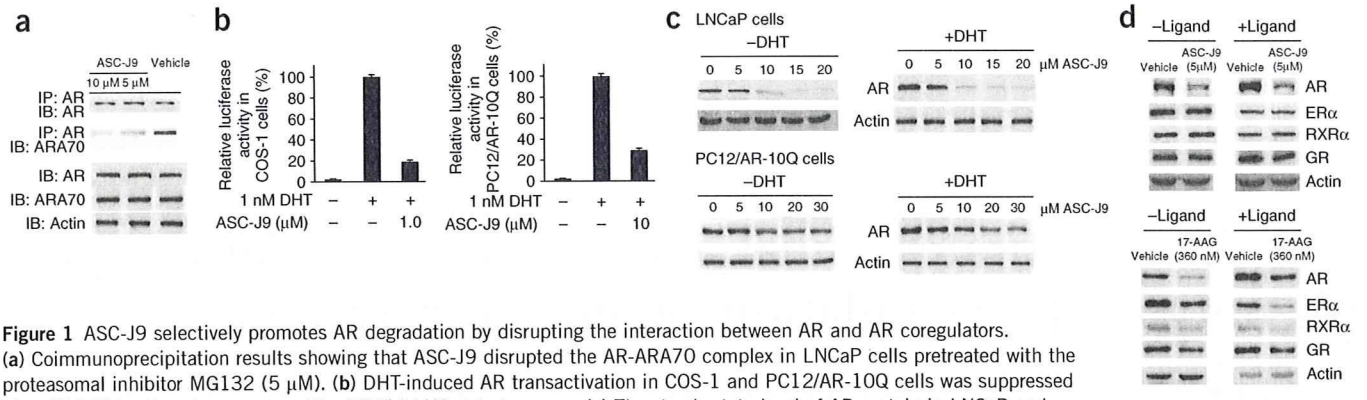

Figure 1 ASC-J9 selectively promotes AR degradation by disrupting the interaction between AR and AR coregulators. (**a**) Coimmunoprecipitation results showing that ASC-J9 disrupted the AR-ARA70 complex in LNCaP cells pretreated with the proteasomal inhibitor MG132 (5 μM). (**b**) DHT-induced AR transactivation in COS-1 and PC12/AR-10Q cells was suppressed after ASC-J9 treatment, as assessed by (ARE)4-LUC reporter assay. (**c**) The steady-state level of AR protein in LNCaP and PC12/AR-10Q cells from western blot assays indicated that the AR signal decreased substantially (in a dose-dependent manner) after treatment with ASC-J9. (**d**) ASC-J9 selectively decreased the steady-state level of AR protein, in the absence and the presence of ligand. In contrast, 17-AAG treatment decreased the steady-state level of all four ligand-activated nuclear receptors (AR, ERα, GR and RXRα), both in the absence and in the presence of the specific ligand.

Moreover, the SBMA mice showed normal sexual activity and improved fertility, suggesting that this strategy might provide a better approach to treating SBMA in men.

RESULTS

ASC-J9 selectively promotes AR degradation

To test our hypothesis that disrupting the interaction between AR and AR-associated proteins is an improved strategy for battling SBMA, we first used a coimmunoprecipitation assay in cultured prostate cancer LNCaP cells, which demonstrated that ASC-J9 promotes the dissociation between AR and its coregulator ARA70 (**Fig. 1a**). We then found that, in COS-1 cells, ASC-J9–induced dissociation between AR and ARA70 led to suppression of AR transactivation (**Fig. 1b**). Similar suppression effects also occurred when we replaced COS-1 cells with PC12/AR-10Q cells (**Fig. 1b**).

To determine whether AR degrades more rapidly when freed of its association with coregulators, we measured the steady-state level of AR protein after the administration of different doses of ASC-J9 in LNCaP and PC12/AR-10Q cells. ASC-J9 treatment decreased the steady-state level of AR protein in the absence and presence of the hormone dihydrotestosterone (DHT), suggesting that ASC-J9 might promote AR protein degradation by disrupting the interaction of AR with AR coregulators (**Fig. 1c**). As the interaction between AR and ARA70 is relatively selective[9], we expected that the degradation of AR by ASC-J9 would also be selective. Whereas ASC-J9 promoted the degradation of AR, it had little effect on other members of the family of ligand-activated nuclear receptors, such as glucocorticoid receptor (GR), estrogen receptor-α (ERα) and retinoid X receptor-α RXRα (**Fig. 1d**). In contrast, the hsp90 inhibitor 17-allylamino-17-demethoxygeldanamycin (17-AAG), which uncouples the interaction between hsp90 and members of this family, unselectively promoted the degradation of AR as well as GR, ERα and RXRα.

Collectively, the results demonstrated that ASC-J9, but not 17-AAG, classic antiandrogen hydroxyflutamide (HF) or curcumin (**Fig. 1d** and **Supplementary Fig. 1** online), can selectively promote AR degradation, which might be secondary to disrupting the interaction between AR and AR coregulators, which results in the suppression of AR transactivation.

ASC-J9 reduces the AR aggregated AR-112Q in cells

The aggregation of AR-polyQ in the nucleus, which is toxic to motor neurons, has been linked to the pathogenesis of SBMA (ref. 11). We tested PC12 cells stably transfected with inducible AR-112Q (PC12/AR-112Q) in a model that mimics the nuclear aggregation present in SBMA (ref. 23) to see whether ASC-J9 can reduce the pathogenesis of SBMA. We found that AR-112Q localized in the cytoplasm in the

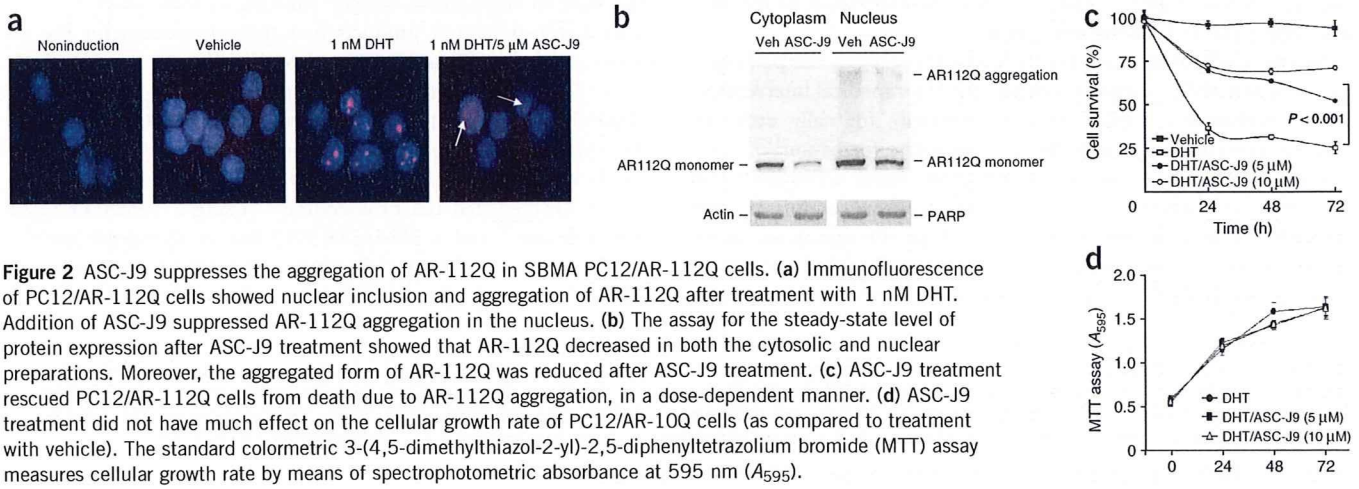

Figure 2 ASC-J9 suppresses the aggregation of AR-112Q in SBMA PC12/AR-112Q cells. (**a**) Immunofluorescence of PC12/AR-112Q cells showed nuclear inclusion and aggregation of AR-112Q after treatment with 1 nM DHT. Addition of ASC-J9 suppressed AR-112Q aggregation in the nucleus. (**b**) The assay for the steady-state level of protein expression after ASC-J9 treatment showed that AR-112Q decreased in both the cytosolic and nuclear preparations. Moreover, the aggregated form of AR-112Q was reduced after ASC-J9 treatment. (**c**) ASC-J9 treatment rescued PC12/AR-112Q cells from death due to AR-112Q aggregation, in a dose-dependent manner. (**d**) ASC-J9 treatment did not have much effect on the cellular growth rate of PC12/AR-10Q cells (as compared to treatment with vehicle). The standard colormetric 3-(4,5-dimethylthiazol-2-yl)-2,5-diphenyltetrazolium bromide (MTT) assay measures cellular growth rate by means of spectrophotometric absorbance at 595 nm (A_{595}).

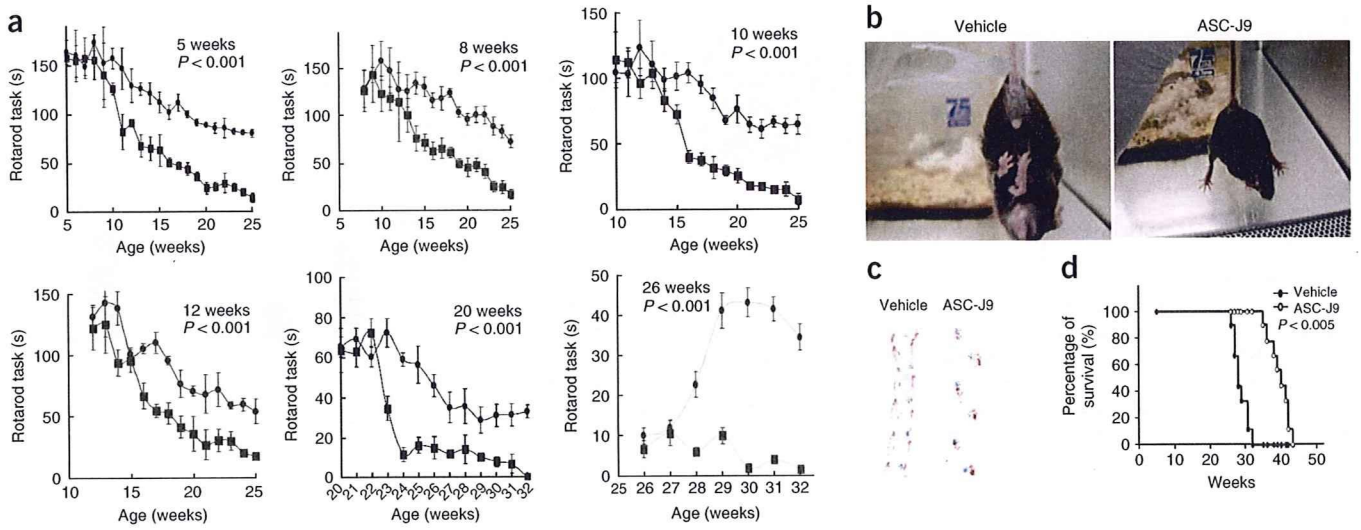

Figure 3 Effects of ASC-J9 (50 mg/kg every 48 h) on SBMA symptoms in male SBMA mice. **(a)** Performance of mice of different ages on the rotarod tasks ($n = 6$ in each group). Mice treated with ASC-J9 showed noticeable improvement even when the treatment started as late as 26 weeks after the onset of SBMA phenotype. **(b–d)** SBMA mice were treated with vehicle or ASC-J9 starting at 5 weeks, and were examined at 15 weeks. With ASC-J9, phenotypic clasping behavior was ameliorated **(b)**, footprint patterns were normal **(c)** and the survival rate had improved **(d)** ($n = 9$ mice in each group). In **c**, front paws are in blue and hind paws in red.

absence of DHT, and addition of 1 nM DHT resulted in the translocation of AR-112Q into the nucleus and subsequent formation of aggregates (**Fig. 2a**). Notably, addition of 5 μM ASC-J9 substantially suppressed the aggregate formation, with little AR-112Q detected in the nucleus (**Fig. 2a**). Western blotting analysis also showed that ASC-J9 treatment promoted the degradation and reduced the amount of aggregated AR-112Q protein in the nucleus (**Fig. 2b**).

In addition, PC12 cell death induced by AR-112Q nuclear aggregation was rescued by the addition of ASC-J9 in a dose-dependent manner (**Fig. 2c**), with little influence on the proliferation of PC12/AR-10Q cells (**Fig. 2d**). Collectively, these results demonstrated that ASC-J9 might reduce cytotoxicity by suppressing the aggregation of AR-112Q in the nucleus and increasing its degradation in the PC12/AR-112Q cells, with little effect on the PC12/AR-10Q cells.

ASC-J9 rescues the SBMA symptoms in AR-97Q mice

We further examined the *in vivo* effects of ASC-J9 in SBMA mice with transgenic AR-97Q (ref. 5). Every other day, we injected male SBMA mice intraperitoneally with ASC-J9 in corn oil at the effective dose of 50 mg per kg body weight, and assessed their motor impairment by testing rotarod activity weekly. We found that the motor impairments were substantially improved in SBMA mice treated with ASC-J9, regardless of whether treatment was started early (at 5 weeks of age) or later (at 26 weeks) (**Fig. 3a**). This observation suggests that ASC-J9 treatment substantially delays the onset and symptomatic progression of motor impairment, which usually appears at 10 weeks. We also found that cage activity increased in SBMA mice treated with ASC-J9 (**Supplementary Video 1** online). The SBMA symptoms of gait disturbance, including severe dragging of hind limbs and erratic footprinting patterns, markedly declined in ASC-J9–treated SBMA mice, suggesting that ASC-J9 treatment can substantially ameliorate the SBMA symptoms in these mice (**Fig. 3b,c**). Notably, ASC-J9 treatment prolonged the lives of these mice, from an average of 28 weeks to 39 weeks (**Fig. 3d**).

Improved sexual functions in SBMA mice treated with ASC-J9

SBMA patients might be reluctant to undergo the helpful but aggressive treatment of surgical or chemical castration because such treatments suppress serum testosterone levels, leading to a loss of normal sexual genital functions and fertility. Notably, we found that ASC-J9–treated SBMA mice had relatively normal serum testosterone concentrations (**Fig. 4a**). Sexual activity, as judged by vaginal plug numbers in female mice caged with the treated males, and fertility, as judged by both pup numbers and litter numbers, were substantially improved during 4 weeks of fertility tests (**Fig. 4b**).

These results demonstrated that there was little adverse influence on serum testosterone and that sexual genital functions and fertility were in fact improved in SBMA mice treated with ASC-J9.

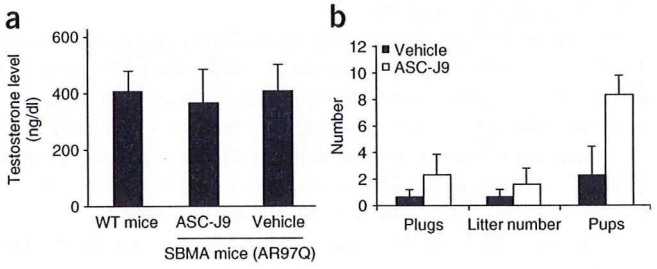

Figure 4 Effect of ASC-J9 (50 mg/kg every 48h) on the fertility and testosterone level of male SBMA mice. We began treatment of SBMA mice at 5 weeks of age. **(a)** We took blood samples from wild-type (WT) and vehicle- or ASC-J9–treated SBMA mice at 20 weeks of age ($n = 9$ mice in each group), and measured serum testosterone levels using an ELISA kit. We found little difference between vehicle- and ASC-J9–treated mice in terms of serum testosterone levels. **(b)** Fertility tests performed on 13-week-old SBMA mice ($n = 4$ mice in each group) showed increased sexual activity following ASC-J9 treatment (compared to vehicle treatment).

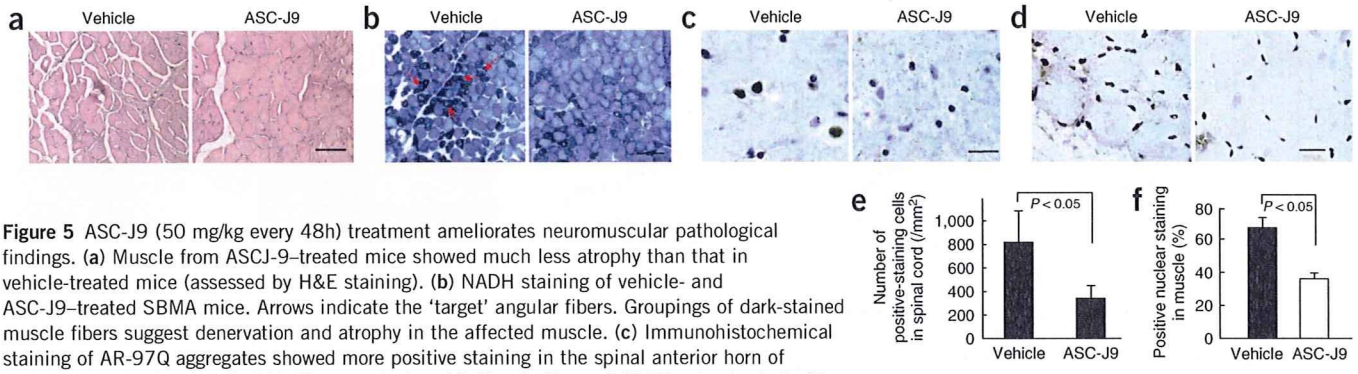

Figure 5 ASC-J9 (50 mg/kg every 48h) treatment ameliorates neuromuscular pathological findings. **(a)** Muscle from ASCJ-9–treated mice showed much less atrophy than that in vehicle-treated mice (assessed by H&E staining). **(b)** NADH staining of vehicle- and ASC-J9–treated SBMA mice. Arrows indicate the 'target' angular fibers. Groupings of dark-stained muscle fibers suggest denervation and atrophy in the affected muscle. **(c)** Immunohistochemical staining of AR-97Q aggregates showed more positive staining in the spinal anterior horn of vehicle-treated mice than in ASC-J9–treated mice. **(d)** Muscle fibers of SBMA mice treated with ASC-J9 showed much less aggregation of AR-112Q than the muscle fibers from vehicle-treated SBMA mice. **(e,f)** There was approximately 50% reduction in AR-aggregated positive-staining cells in the spinal cord and the muscle fibers after ASC-J9 treatment compared with vehicle treatment. Scale bars: 100 μm in **a** and **b**, 20 μm in **c** and **d**.

ASC-J9 reverses muscular atrophy and restores VEGF expression

Hematoxylin and eosin staining showed that ASC-J9 treatment substantially reduced muscular atrophy compared to vehicle treatment (**Fig. 5a**). By using nicotinamide adenine dinucleotide (NADH) to stain muscle, we also found that the groupings of muscle fibers were markedly altered in the ASC-J9–treated mice (**Fig. 5b**). There were more groupings of ankylated muscle fibers, suggesting the denervation and atrophy of muscle fibers, in vehicle-treated mice than in ASC-J9–treated mice (**Fig. 5b**). Immunohistochemical staining using an antibody to AR, N20, showed the intranuclear aggregation of AR-97Q in spinal cord motor neurons and skeletal muscle cells (**Fig. 5c,d**). Also, the intranuclear AR-97Q aggregation in spinal cord neurons and muscle cells was significantly lower (by almost 50%) in the ASC-J9–treated mice than in the vehicle-treated mice (**Fig. 5e,f**).

Motor neuron survival and proper function requires VEGF164 expression. Previous studies have suggested that aggregated AR-97Q might associate abnormally with CBP, resulting in the disruption of CBP-mediated VEGF164 expression[24]. By examining coimmunoprecipitation in PC12/AR-112Q and PC12/AR-Q10 cells, we found that ASC-J9 dose-dependently disrupted the interaction between AR-112Q and CBP in PC12/AR-112Q cells but had little influence in PC12/AR-10Q cells (**Fig. 6a**). Releasing CBP from its interaction with AR-112Q in PC12/AR-112Q cells was associated with the induction of VEGF164 expression (**Fig. 6b**).

We further confirmed this finding by showing a significant increase (from 20% to 90%) in the expression of mRNA for VEGF164 in the spinal cord of SBMA mice following ASC-J9 treatment (**Fig. 6c**). Moreover, the ELISA assay to detect the levels of VEGF protein in the spinal cord of these mice also demonstrated a significant increase of VEGF expression after ASC-J9 treatment (**Fig. 6d**). These results do not formally prove that ASC-J9 ameliorates SBMA symptoms by restoring VEGF164 expression, but they are consistent with this idea.

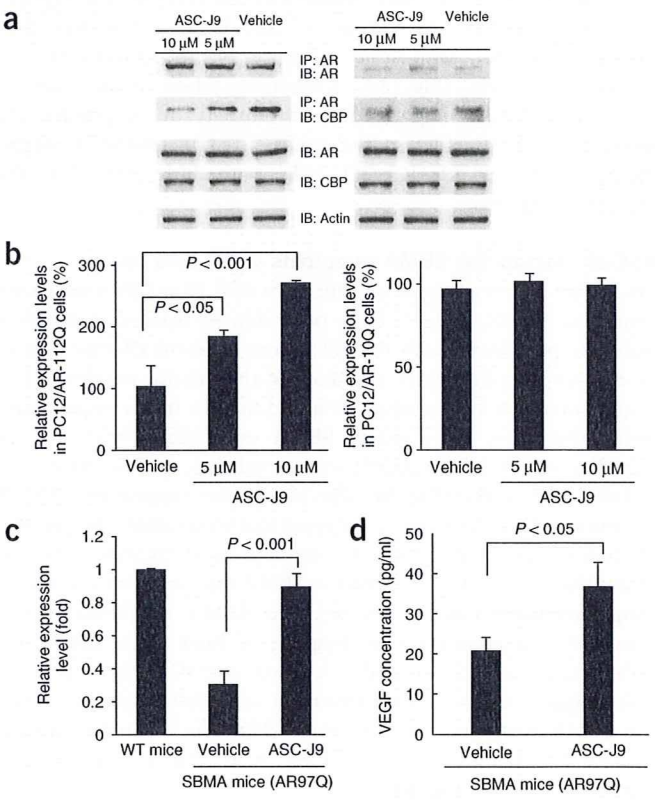

Figure 6 Molecular mechanisms of the effect of ASC-J9 on the SBMA phenotypes. **(a)** Treatment with 5 μM or 10 μM ASC-J9 showed dose-dependent disruption of the interaction between CBP and AR-112Q or AR-10Q in PC12 cells pretreated with the proteasomal inhibitor MG132 (5 μM). **(b)** ASC-J9 treatment increased VEGF164 expression in PC12/AR-112Q cells but had little influence in PC12/AR-10Q cells pretreated with MG132. **(c)** ASC-J9 treatment had a dose-dependent effect on increasing mRNA for VEGF164 in the spinal cord. **(d)** Amounts of VEGF protein from homogenized L5 spinal cords were increased after ASC-J9 treatment.

DISCUSSION

It has been shown that one of hsp90's associated proteins, AR, can be degraded when the interaction between hsp90 and its associated proteins is disrupted by using the hsp90 inhibitor 17-AAG. This degradation reduces the longer AR-97Q nuclear aggregates in SBMA mice[25]. However, 17-AAG also disrupts the interaction between hsp90 and many other proteins, including GR, ERα and RXRα (**Fig. 1d**), and Her2, Her3 receptor tyrosine kinase, Erk1/2 and Rb (refs. 25–30), rendering them more susceptible to degradation. Recent reports have clearly documented that common adverse reactions to 17-AAG include anorexia, diarrhea, nausea, fatigue and vomiting, along with the reversible elevation of liver enzymes (in 29.5% of subjects)[31]. This inhibitor also enhances bone metastasis and osteolytic lesions, which

lead to increased osteolysis and incidence of skeletal tumors[32]. The nonspecific disruption by 17-AAG of the interaction between hsp90 and most of its associated proteins leads to extensive adverse and unwanted side effects, and therefore limits the applicability of 17-AAG in the treatment of SBMA. In contrast, ASC-J9 (at a dose of 50 mg/kg every 48 h for more than 20 weeks) had no obvious toxic effects and did not result in a loss of body weight in mice. Moreover, the sexual genital functions and fertility in these SBMA mice were improved markedly. Together, these positive results of ASC-J9 treatment demonstrate that this new approach—involving the selective disruption of interactions between AR-polyQ and AR coregulators, such as CBP—might offer improved treatment for SBMA. Additional dosage studies of ASC-J9 or its derivatives to investigate how SBMA symptoms may be effectively ameliorated, without toxicity, might lead to treatments that could substantially improve the quality of life of SBMA patients.

METHODS

Therapeutic agent and administration protocol. ASC-J9 from AndroScience was synthesized as described previously[22]. We dissolved it in corn oil and injected it intraperitoneally into mice (50 mg/kg every other day) at various ages until the end of the study. Control mice received DMSO in corn oil only.

ASC-J9 characterization. For the AR degradation study, we treated LNCaP cells with vehicle and 1 nM DHT with or without 5 μM ASC-J9, in RPMI supplemented with 10% charcoal dextran–stripped (CDS) FBS. At selected time intervals, we harvested cells and analyzed AR protein levels by western blotting, quantitated the results by Bio-Rad PDQuest Image software, and normalized densitometric values to actin. We purchased the antibodies for AR (N20), CBP (C-1), ERα (HC-20), GR (P-20), RXRα (D-20), CBP, PARP and actin from Santa Cruz Biotechnology and generated ARA70 antibody as previously described[33].

For the AR-112Q protein steady-state assay, we cultured PC12/AR-112Q cells as described previously[23], in the presence of 10 μg/ml doxycycline for 24 h, and then treated cells with or without 1 nM DHT or 1 nM DHT and 5 μM ASC-J9 for 3 d. We performed the cytosolic and nuclear extraction by FractionPREP™ Cell Fraction System (BioVision) and analyzed the AR-112Q by western blotting.

We performed the protein steady-state assay of AR, GR, ERα and RXRα in response to 5 μM ASC-J9 or 360 nM 17-AAG, on LNCaP cells (AR and RXRα), MCF-7 cells (ERα) and PC3 cells (GR), in the presence or absence of ligand (1 nM DHT for AR, 1 nM E2 for ERα, 1 nM dexamethasone for GR and 1 μM 9-cis-RA for RXRα). We determined the amounts of AR, GR, ERα and RXRα proteins by western blotting and analyzed the interactions between AR-ARA70 complex and AR-CBP complex by coimmunoprecipitation[24,33]. We assayed AR transactivation activity as described previously[34].

Immunofluorescence staining and cell survival. We cultured PC12/AR-112Q cells in two-well Chamber slides (Nalge Nunc) supplemented by DMEM, 10% CDS horse serum and 100 μg/ml nerve growth factor (BD Biosciences), and induced AR-112Q by 10 μg/ml doxycycline (Sigma) for 4 h. Then we treated cells with vehicle, 1 nM DHT, or 1 nm DHT and 5 μM ASC-J9 for 3 d. We stained AR-112Q with N20 antibody and Texas Red–conjugated streptavidin (Vector Laboratories), mounted slides in fluorescent mounting medium containing 4′,6-diamidino-2-phenylindole (DAPI), and observed fluorescent staining using an Olympus fluorescent microscope.

For the cell survival assay, we cultured PC12/AR-112Q and PC12/AR-10Q cells as described previously[23] and incubated cells in the presence of 10 μg/ml doxycycline for 24 h. Then we treated cells with vehicle, 5 μM ASC-J9 or 10 μM ASC-J9, along with 1 nM DHT, and determined cell viability using Trypan blue staining at specific time intervals.

SBMA mouse model generation, maintenance, genotyping and motor activity assessment. We generated the AR-97Q SBMA mice as described previously[5]. We performed all animal experiments in accordance with the Guide for the Care and Use of Laboratory Animals of the US National Institutes of Health and with approval from the Department of Laboratory Animal Medicine at the University of Rochester. We assessed rotarod performance weekly using an Economex Rotarod (Colombus Instruments) as described[35], and observed footprints for ASC-J9– or vehicle-treated SBMA mice by dipping their forepaws in water-soluble red paint and hind paws in blue paint. The mice then walked through a narrow tunnel, leaving footprints on a strip of white paper[21].

Serum testosterone and male fertility. We killed SBMA mice receiving ASC-J9 or vehicle treatment at 20 weeks of age, drew 1 ml of blood by cardiocentesis, and assayed serum testosterone with the Coat-A-Count Total Testosterone radioimmunoassay (Diagnostic Products) according to the manufacturer's protocol. We observed the reproductive capacities of ASC-J9 and vehicle-treated SBMA mice by mating one male mouse with two B6 female mice for 1 week checking female mice for vaginal plugs each morning and recording litter sizes on delivery after four successive matings.

Histology and immunohistochemistry. We fixed tissues by 4% paraformaldehyde and embedded them in paraffin. For general histologic inspection, we treated tissue sections with H&E or NADH, and then used an ABC kit (Vector Laboratories) to detect AR immunostaining by an N20 antibody to AR. We performed the assessment of cells with intranuclear aggregated AR-polyQ in the ventral horn of the spinal cord as described previously[36,37]. We expressed the populations of AR-positive cells as the number per square millimeter. We counted AR-positive cells in randomly selected areas from more than 500 muscle fibers and expressed AR-positive cells as the number per 100 muscle fibers.

Quantitative real time RT-PCR. We harvested L5 spinal cords of mice treated with vehicle or ASC-J9 (50 mg/kg every 48 h), extracted total RNA using TRIZOL and reverse transcribed. We subjected 1 μg of total RNA to reverse transcription using Superscript II (Invitrogen), with the primer probe sequences and PCR conditions for VEGF164 as described previously[24]. We performed amplification, detection, and data analysis using a Bio-Rad iCycler system.

ELISA. We obtained total protein lysates by homogenizing tissues in an extraction buffer as described previously[24]. After centrifugation, we analyzed the amount of VEGF protein in the supernatant using ELISA kit (R&D Systems).

Statistical analysis. We analyzed the results by unpaired *t*-tests and log-rank tests for survival rate using Sigmaplot software. *P*-values less than 0.05 were considered to be statistically significant.

Note: Supplementary information is available on the Nature Medicine website.

ACKNOWLEDGMENTS

We thank K. Wolf for help in editing the manuscript. This work was supported by US National Institutes of Health grant DK067686 and the George Whipple Professorship Endowment.

COMPETING INTERESTS STATEMENT

The authors declare competing financial interests (see the *Nature Medicine* website for details).

Published online at http://www.nature.com/naturemedicine
Reprints and permissions information is available online at http://npg.nature.com/reprintsandpermissions

1. Kennedy, W.R., Alter, M. & Sung, J.H. Progressive proximal spinal and bulbar muscular atrophy of late onset: a sex-linked recessive trait. *Neurology* **50**, 583–593 (1998).
2. La Spada, A.R., Wilson, E.M., Lubahn, D.B., Harding, A.E. & Fischbeck, K.H. Androgen receptor gene mutations in X-linked spinal and bulbar muscular atrophy. *Nature* **352**, 77–79 (1991).
3. Ringel, S.P., Lava, N.S., Treihaft, M.M., Lubs, M.L. & Lubs, H.A. Late-onset X-linked recessive spinal and bulbar muscular atrophy. *Muscle Nerve* **1**, 297–307 (1978).
4. Sobue, G. *et al.* X-linked recessive bulbospinal neuronopathy. A clinicopathological study. *Brain* **112**, 209–232 (1989).
5. Katsuno, M. *et al.* Testosterone reduction prevents phenotypic expression in a transgenic mouse model of spinal and bulbar muscular atrophy. *Neuron* **35**, 843–854 (2002).
6. Li, M. *et al.* Nuclear inclusions of the androgen receptor protein in spinal and bulbar muscular atrophy. *Ann. Neurol.* **44**, 249–254 (1998).